Extreme convective gusts in a future warmer climate assessed through a convection permitting model

Camilla Cecilia van Wirdum

TUDelft

Master Thesis Report

Extreme convective gusts in a future warmer climate assessed through
a convection permitting model

October 23$^{\text{rd}}$ 2020
To be defended publicly on November 3$^{\text{rd}}$ 2020 at 2:45 pm

by

Camilla Cecilia van Wirdum

in partial fulfillment to obtain the degree of Master of Science
at the Delft University of Technology

Student number:	4367871	
Project duration:	December 1$^{\text{st}}$ 2019 – October 23$^{\text{rd}}$ 2020	
Thesis committee:	Dr. S. Basu	TU Delft chair
	Ir. C. M. H. Unal	TU Delft
	Dr. Ir. G. Lenderink	TU Delft, KNMI
	Dr. A. Sterl	KNMI
	Dr. H. de Vries	KNMI

Abstract

Severe wind gusts associated with mid-latitude convective storms contribute to an increasing amount of natural hazard related losses in Europe. Modifications of the atmosphere associated with anthropogenic climate change are projected to increase the frequency of favorable conditions for convective storms, and it is absolutely critical to understand the implications of these changes to prepare for a resilient future. To this end, the fate of convective gusts in Europe in a future warmer climate is addressed through the output of two high resolution regional climate models (RCMs). One RCM includes convection permitting (CP) physics, and the other assumes hydrostatic conditions in which deep convection is parameterized. It is found that the magnitude and characteristics of extreme straight line gusts from mesoscale convective systems are well resolved in the CP-RCM but not in the hydrostatic RCM. The RCMs are forced with a high carbon emission scenario for the end of the 21st century, and the CP-RCM shows an increase in the frequency and magnitude of extreme convective gusts over mainland Europe. These changes are likely related to an increase in conditions where strong wind shear (≥ 15 m/s) simultaneously occurs with unstable environments (lifted index ≤ -2). However, the inherent low frequency of extreme convective storms requires continued investigation to draw more robust conclusions. In addition, the environmental conditions in which the severe gusts take place indicate the importance of addressing gusts separately from the more commonly studied effects of climate change on extreme convective precipitation. This thesis provides an important bridge to understand the fate of extreme gusts from convective storms in a future warmer climate and the high potential of CP-RCMs in such studies.

Preface

This thesis is the final work of my time as a university student. It has been a wonderful journey that allowed me to get to know the world through unforgettable adventures around the globe. Studying the Earth and her wondrous processes has been the guiding theme throughout my years at university. After studying what processes formed and govern our planet, this thesis provides an introduction into how we are changing it and what challenges await us in the future. The project is part of the Royal Netherlands Meteorological Institute (KNMI) Climate Scenarios that give insight into the future climate of the Netherlands. Non-technical summaries of this report in Dutch and English can be found on www.camillacecilia.com/thesis. This all would not have been possible without all the wonderful people I am surrounded with. I am especially grateful to my parents and family, who have let me explore the things I love and who I want to be with limitless support.

A big thank you to Andreas and Hylke for giving me the opportunity to work with KNMI and their guidance in the process of researching and writing my thesis. Your detailed feedback and mentoring has been very valuable. To Sukanta, who has shown to be a wonderful teacher, ready to help and to provide rigorous feedback. To the other committee members, Geert and Christine, each of whom has provided patient advice and guidance in the process. To the KNMI colleagues, each with their own valuable expertise open for any questions I had.

To Thomas for his patience and keeping me sane whilst working together in this extraordinary year, with heatwaves and a global pandemic, accompanied with the struggles that come with nearing the end of time as a student. To Dylan for his critical view, proofreading and for sharing the best moments of my master program together. To all my friends, for without your interest, in clouds in particular, the writing of my thesis would have been a lot less fun.

I have no doubt I will continue exploring and learning after my time in university. I cannot wait to put all that I have learned over the last years in practice in a career that will aim to make our planet and her inhabitants more resilient for the future.

C.C. van Wirdum
Amsterdam, October 2020

Contents

List of Acronyms

Acronym	Description
CAPE	Convective available potential energy
CIN	Convective inhibition
CP	Convection permitting
DMC	Deep moist convection
ECMWF	European Centre for Medium-Range Weather Forecasts
EOC	End of century (2090-2099)
f_{20}, f_{25}	Frequency of days above 20 m/s and 25 m/s, respectively
GCM	General circulation model
GPD	General Pareto distribution
HClim	Harmonie Climate, a convection permitting regional climate model (Belušić et al., 2020)
HClim-ERA	Harmonie Climate, forced with ERA-interim (2000-2009)
hist	History (1996-2005)
IPCC	Intergovernmental Panel on Climate Change
KNMI	Royal Netherlands Meteorological Institute
LI	Lifted index, measure for atmospheric instability
LFC	Level of free convection
MBE	Mean bias error
MOC	Mid of century (2041-2050)
MCS	Mesoscale convective system
POT	Peak over threshold method for extreme value analysis
p_{95}, p_{99}	The 95th and 99th percentile of data, respectively
RCM	Regional climate model
RCP	Representative concentration pathway, emission scenarios of the IPCC
RL_{10}, RL_{50}	Return levels belonging to a return period of 10 and 50 years, respectively
RMSE	Root mean squared error
TD2m	Dew point temperature 2 meters above the surface
TKE	Turbulent kinetic energy
WMO	World Meteorological Organisation

List of Figures

The image on the front page is used with the permission of photographer Peter Maier, 2018.

List of Tables

Chapter 1

Introduction

1.1   Background

Severe convective storms are a major natural hazard as they are commonly paired with strong gusts, hail, lightning, flooding and tornadoes. Per year, convective storms are responsible for an estimated 5 to 8 billion euros damage for European countries (Munich Re Group, Dotzek et al., 2009). To this end, it is of major importance to understand how convective storms will change in a warming climate for the development of adaptation strategies for amongst others the wind energy sector, transportation links, forestry and coastal protection. Recently, an increasing number of studies have addressed the implications of warmer temperatures for extreme convective precipitation (for example, Kendon et al., 2017, Lenderink et al., 2019 and Vanden Broucke et al., 2019). In addition, several studies have confirmed an increase in favorable conditions for extreme convective weather in a future warmer climate (Rädler et al., 2019; Púčik et al., 2017 and Diffenbaugh et al., 2013). Such studies, however, have not been done so far for convective gusts specifically, and their response to elevated greenhouse forcing remains highly uncertain. One major reason for the lack of understanding is the local and short-lived nature of convective storms and the associated challenges to represent them in climate models. Fortunately, increasing computational power has led to the development of high resolution convection permitting (CP) regional climate models (RCMs) that have the potential of resolving such phenomena.

1.2   Research objectives

The main objective of this thesis is to address how extreme gusts associated with convective storms are projected to change in a future warmer climate through a CP-RCM in Europe (objective C, see section 1.4 and Figure 1.1 for overviews). Before this can be addressed, it is vital to understand how convective storms form, what the key ingredients are for the development of extreme gusts, how their environmental conditions are expected to change and how they can be represented in climate models. To this end, objective A is designed.

In traditional RCMs, the resolution is too coarse to resolve deep convection explicitly, and parameterization schemes are applied. These schemes are often thought to be a major source of uncertainty, and hence CP-RCMs have been developed with the capability of resolving deep convection explicitly. This however comes at high computational costs, and it is important to explore what the actual added value is. The ability CP-RCMs to represent extreme convective precipita-
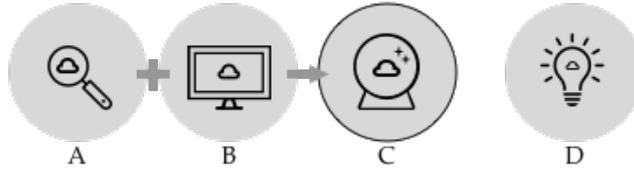
Figure 1.1: *The four research objectives visualized. The main objective is to investigate how convective gusts are projected to change in a future warmer climate in Europe through a CP-RCM (objective C). To this end, it is important to first understand the theory behind the formation and key ingredients of extreme gusts in convective storms and how they can be represented in climate models (objective A). Objective B addresses the ability of CP-RCMs to resolve extreme convective gusts. Finally, objective D aims to expose any remaining knowledge gaps and make recommendations for further research.*

tion is addressed extensively in literature (for example, Kendon et al., 2017, Prein et al., 2015 and Vanden Broucke et al., 2019), and it was found that the benefits lie mainly in statistics related to deep convection, complex terrain and extreme events (Prein et al., 2015), though the results strongly depend on timescale and topography (Vanden Broucke et al., 2019). The ability of CP-RCMs to resolve extreme convective gusts accurately remains largely unaddressed. To this end, objective B is designed. The results from objectives A, B and C are used to identify remaining knowledge gaps and to make recommendations for future studies as addressed in objective D.

1.3   Research approach and scope

This thesis commences with an extensive literature overview on the formation, key ingredients and projections of the environmental conditions in a warmer climate of extreme convective gusts as well as methods to represent them in regional climate models in chapter 2. In chapters 3 and 4 the data used and methodology are further discussed. In short, the CP-RCM output for this thesis comes from the high resolution (app. 2.5 km) model Harmonie Climate (HClim, Belušić et al., 2020). HClim takes its boundary conditions from the hydrostatic RCM RACMO (ECMWF, 2009), which in turn is forced by the general circulation model (GCM) EC-Earth (Hazeleger et al., 2012). In addition to the EC-Earth runs, one evaluation run is forced with the global atmospheric reanalysis product ERA-interim (Dee et al., 2011) to allow an assessment of the performance of the EC-Earth driven runs. To evaluate the ability of the CP-RCM to resolve convective gusts, observational data from 22 meteorological stations from the Royal Netherlands Meteorological Institute (KNMI) are utilized.

This study additionally investigates whether it is possible to use the traditional and coarser resolution RACMO output directly to investigate the changes to extreme wind gusts in a future climate. RACMO data without downscaling by HClim is available for the entire 21st century (Van Meijgaard et al., 2012). The HClim downscaled runs are available for a historical period, and for the middle and end of the 21st century for a large part of the European continent. In EC-Earth a high carbon emission scenario from the Intergovernmental Panel on Climate Change (IPCC) is incorporated to explore the effects of anthropogenic climate change. The performance of the models for gusts and the behaviour of extreme convective gusts in a future warmer climate is addressed through two lenses. The first is a climatological approach, and in the second case studies are selected to investigate the dynamical aspects of the performance and future changes in more detail. The objectives of this thesis are addressed through the research questions given on the next page.

1.4 Research questions

Part A: understand key ingredients for extreme convective gusts, their projections and how convective storms can be represented in models

A1. How are convection-induced gusts and their environmental indicators expected to change in a warming climate theoretically?

A2. What methods can be used to parameterize gusts and how do the methods of HClim and RACMO compare?

Part B: explore whether convection permitting regional climate models are effective for studying convective gusts

B1. How well are convective gusts represented in HClim compared to observational data in the Netherlands?

B2. How does the EC-Earth forced historical HClim run perform compared to the HClim ERA-interim run?

B3. Can the same results of the CP-RCM be obtained using the coarser and hydrostatic RCM RACMO?

Part C: investigate how convective gusts will change in a future warmer climate

C1. From a climatology standpoint, how are convection-induced wind gusts expected to change in a warming climate?

C2. From a dynamical perspective, how are convection-induced wind gusts expected to change in a warming climate?

Part D: recommend further investigation and explore what knowledge gaps remain

D1. Are there important remaining knowledge gaps regarding how convective gusts might respond to climate change?

Chapter 2

Convective Gusts

This chapter provides an overview of the theory behind the formation, development and key ingredients for convective storms paired with severe gusts and briefly discusses how the ingredients are expected to change in a future warmer climate (objective A1). Next, methods to represent convection and convective gusts in weather and climate models through parameterization schemes are discussed, as well as the effect of model resolution on their representation (objective A2).

2.1 Formation of isolated convective storms

Extreme convective gusts form as result of downdrafts from isolated and organised convective storms. Extreme convective storms require specific environmental conditions, usually including the presence of moisture, instability and a source of upward motion. In addition, strong vertical wind shear is required for a convective structure to become more organised and to produce severe winds. Understanding the formation and dynamics of isolated storms is important as they form the building blocks of more complicated mesoscale convective systems producing severe winds, such as squall lines and mesoscale convective complexes.

In literature, various methods have been proposed to classify storms based on their internal structure, rainfall intensity, potential severity, longevity and propagation characteristics. This text adapts the same nomenclature as the books of Lin (2007) and Markowski and Richardson (2011), where isolated storms are categorized as single-cell, multicell and supercell storms.

Single-cell storms occur in situations with weak wind shear and abundant moisture, and often have a short lifetime (30-50 minutes). In situations with moderate shear, multiple single-cells at various stages can form a multicell storm. These storms last longer as new cells continue to develop along the gust front while older cells dissipate. When shear is even stronger, a much longer lived supercell can form that consists of a single rotating updraft. This last type often produces the majority of severe weather. The next sections discuss the three types of isolated storms, as well as the organization of them into larger systems.

2.1.1 Dynamics of single-cell storms

Of the three isolated storm types, the dynamics of single-cell storms are best understood due to their less complicated dynamics. The formation of a single-cell storm can be summarized in three steps. In the developing stage, air parcels rise by latent heat release, resulting in towering cumulus clouds (Figure 2.1a). The process of air being lifted to saturation, subsequently achieving positive

buoyancy and rising to great heights is also referred to as deep moist convection (DMC; Markowski and Richardson, 2011). In the upward journey rain drops or ice particles form in the upper portion of the cumulus clouds. In the mature stage (Figure 2.1b) the cloud continues to grow and precipitation starts to fall below the cloud base. The evaporation from the descending precipitation cools the unsaturated air underneath the cloud base to form a cold pool. Due to hydrostatics, this in turn leads to a mesoscale region of high pressure near the surface. The mass of cold air descending is also known as a cold pool or downdraft, see Figure 2.2 for a visualisation, and can be up to a few kilometers in size. When the cold air mass hits the Earth's surface, it is deflected, cutting the inflow of warm air into the updraft in case of weak shear (often ≤ 10 m/s in the lowest 4 km, Markowski and Richardson, 2011), resulting in a dissipating stage of the storm (Figure 2.1c). For this reason, single-cell storms are usually not strong enough and too short-lived to produce severe weather.
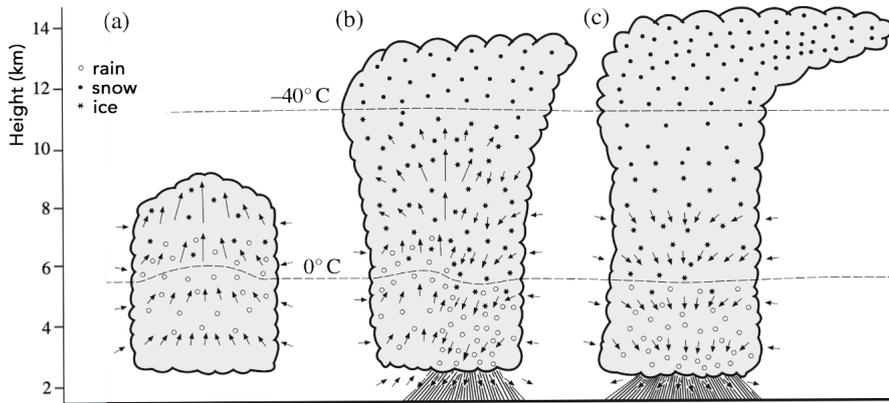
Figure 2.1: *Schematic overview of the (a) developing (b) mature and (c) dissipating stage of a single-cell storm. Adapted from Lin (2007), chapter 8.*

2.1.2 Downdrafts and downbursts

In case a strong downdraft induces a large area of damaging winds in the proximity of the Earth's surface it is referred to as a downburst. To differentiate gust fronts and severe winds associated with downbursts from the rotating nature of winds associated with tornadoes, they are often named straight-line winds. According to their size, intensity and characteristics, downbursts can be further classified into macrobursts and microbursts. Marcobrusts are downbursts with a spatial extent of more than 4 km and last for 5 to 30 minutes, whereas microbusts are smaller than 4 km and last anywhere between 2 to 5 minutes. In its turn, microbursts can be further classified into dry and wet microbursts (Fujita and Wakimoto, 1983). Dry microbursts are paired with little or no precipitation during their downwards journey, whereas wet microbursts are often accompanied by heavy precipitation (see Figure 2.2 for an example).

2.1.3 Dynamics of multicell storms

Multicell storms consist of a cluster of convective cells that are at different stages in their life cycles and can develop in conditions with increased vertical wind shear. See section 2.2.2 for a more detailed description on the influence of shear on convective storm development. The key for genesis

Figure 2.2: *Photograph of a summer storm taken in the proximity of Tilburg, the Netherlands, on the 29th of June 2020, by Jan van Hoof. The descending air paired with precipitation, also known as a cold pool, downdraft or downburst, is clearly visible. In this case, the spatial extent of the downburst is less than 4 km and associated with precipitation, and is therefore also referred to as a wet microburst.*

of multicells is the development of new convective cells around the boundary of the cold pool outflow, also called the gust front. At this location the new cell develops vertically and moves rearward in the front-to-rear (FTR) jet. The FTR jet is an ascending airflow coming from the surface and residing above the cold pool and moves towards the rear side of the storm and over the rear-to-front (RTF) jet. The RTF jet flows from the rear part of a storm towards the rear part of the cold pool. Both jets are shown with bold stream lines in Figure 2.3. In a process repeating every 10 to 15 minutes, after the new cells are developed, they are cut off from the gust front updraft. In case of weak shear, the up- and downdrafts would take place in close proximity, and hence dissipating one another to some extent. Due to the stronger shear, new cells are able to develop making a more sustained system.

A series of convective cells in various stages of their life cycles is represented by n - 2 to n + 1 as depicted in Figure 2.3. The n - 2 cell is in a decaying stage, and has weak down- and updrafts at most levels. Cell n - 1 is in a mature stage and has almost reached maximum intensity. Cell n is in a developing stage, growing from the gust front. The gust front often comes paired with the horizontally protruding shelf cloud, as captured in Figure 2.4. The newest cell n + 1 is around 15 minutes behind the shelf cloud of the n cell. The life cycle of one cell is around 1 hour.

2.1.4 Dynamics of supercell storms

In case of strong vertical wind shear, a convective storm can possess a persistent, deep, rotating updraft, and the storm in such case is referred to as a supercell storm. A mesocyclone, a cyclonically rotating vortex with a diameter of 2 to 10 km, is often embedded in a supercell storm. Supercell
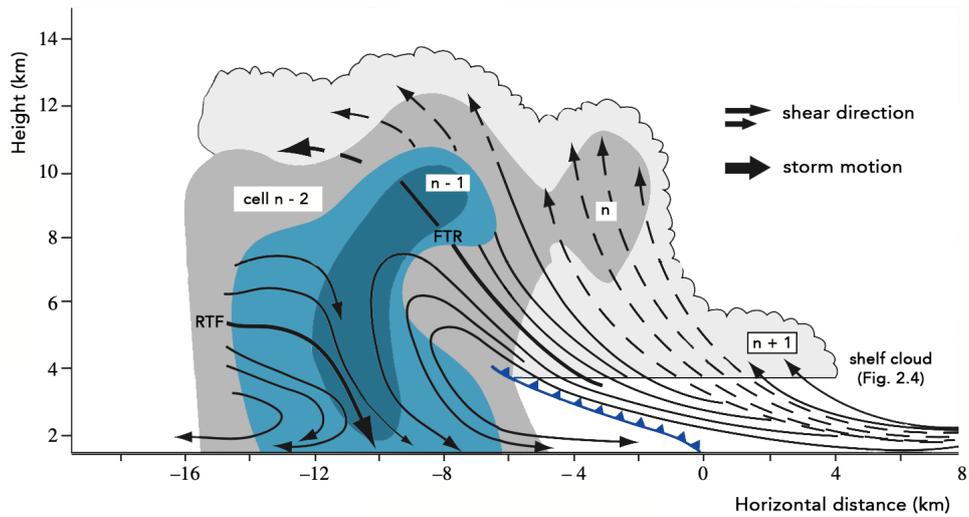
Figure 2.3: *Schematic visualization of a multicell storm, in the vertical plane along the direction of the storm's movement. The storm consist of four cells: $n-2$ to $n+1$, that were generated at the gust front and moved to the left as they developed. The front-to-rear and rear-to-front jets are denoted by FTR and RTF, respectively. Adapted from Lin (2007), chapter 8, and Browning and Foote (1976).*

Figure 2.4: *Shelf cloud associated with a convective storm front approaching Utrecht, the Netherlands in the late afternoon of the 16th of August 2020. Image taken by Pieter Groot Bramel.*

storms often move along the direction of the mean environmental wind, and tend to last for several hours due to the strong vertical shear. Although similar in size compared to multicell storms, the

cloud structure, flow structure, flow circulation and formation of precipitation are organized by a single massive updraft-downdraft pair. Supercells tend to result in the most intense and long-lasting tornadoes and damaging hail, and are governed by complicated physical processes (Markowski and Richardson, 2011). The updraft speeds of up to 40 m/s of supercells are significantly higher than those of single-cell and multicell storms.

2.1.5 Tornadoes and waterspouts

Tornadoes are rapidly rotating columns of air, and often extend downwards from the base of a cumulonimbus updraft in supercells storms (see Figure 2.5). When a tornado occurs over sea, it is often referred to as a waterspout. The damage caused by tornadoes locally cannot be found in the most severe larger scale storms, though their catastrophic footprint typically extends only a few hundred meters wide and last only around 10 minutes. In Europe, around 170 tornadoes are observed yearly, and around 300 take place based on estimates (Dotzek, 2003). A significant proportion of these occur in the Netherlands, with 20 observed and 35 estimated yearly (Dotzek, 2003). This is the highest amount in Europe after the United Kingdom (Dotzek, 2003). In terms of waterspouts the Netherlands have by far the highest number in Europe with 60 observed and 100 estimated, mostly due to the climatology of the North Sea coastal plains (Dotzek, 2003). Tornadoes can be associated with any form of DMC, though the most violent tornadoes are associated with supercell storms, or in environments where the 0 to 6 km shear is at minimum 20 m/s and CAPE $\geq$ 1000 J/kg (Brooks et al., 2003). Two of the most discriminating proxies for predicting if a supercell produces tornadoes are large boundary layer relative humidity and the low-level vertical wind shear (Markowski and Richardson, 2011). The study of Thompson et al. (2003) examined more than 400 soundings of both tornadic and nontornadic supercells in relation to their environmental conditions. They found that the most significant discriminator between tornadic and nontornadic supercells is low vertical shear (0-1 km) and moisture within 1 km from the ground. For distinction between supercell environments to non-supercell environments, the wind shear between the surface and 6 km is still reported most powerful (Thompson et al., 2003). Despite the findings of Thompson et al. (2003), tornadoes are still often thought to be 'mesoscale accidents', that is, there is a strong random element to tornado formation within supercells (Markowski and Richardson, 2011).

2.1.6 Formation of mesoscale convective systems

The isolated convective storms, as discussed in the previous section, form the building blocks for mesoscale convective systems (MCSs). According to the definition of the American Meteorological Society, the horizontal scale of MCSs is at least 100 km at midlatitudes and have a lifetime of around 3 hours or more. At these scales, Coriolis acceleration plays a significant role in the dynamics of MCSs. MCSs can start to form from convection that is somewhat isolated, and can develop in a process commonly called upscale growth. In this process, outflows from isolated storms tend to merge into a single, widespread cold pool. This large cold pool is in turn able to grow new cells at its convection-initiating boundary. Upscale growth is enhanced in environments where deep-layer wind shear has a major component parallel to the gust front (Markowski and Richardson, 2011). In other instances, MCSs can develop almost immediately after convective initiation, especially in environments with low convective inhibition (see section 2.2.1). Most MCSs can be regarded as multicell storms (see section 2.1.3), as new cells are continuously generated in the gust front. The structure of many MCSs therefore closely resembles the schematic of 2.3 when extended into and out of the page.

Figure 2.5: *Tornado in Amsterdam on August 9th, 2019 (nu.nl, 2019).*

Organised MCSs can increase the likelihood of severe surface winds in multiple ways. First, mesoscale cold pools can be generated when the outflow of multiple isolated storms merge. This process causes mesoscale pressure gradients, that in turn can result in severe winds without the presence of downdrafts. Second, the same cold pools can strengthen convective redevelopment in environments already supportive of intense downdrafts. And third, the internal dynamics of MCSs can result in local strengthening of gusts when a rear-inflow yet reaches the surface and takes along large horizontal momentum (Weisman and Klemp, 1982). MCSs can be subclassified in multiple ways, and a first distinction is often made between squall lines and mesoscale convective complexes (MCCs) in the midlatitudes, and tropical storms (cyclones) and cloud clusters at tropical latitudes. Squall lines are MCSs that consist of an organized line of thunderstorms created by deep convective cells on a scale between 1 to 10 km. In some cases, bow echos are visible as arc-shaped structures within squall lines. MCCs have a more circular anvil shape compared to squall lines and occur in environments with low wind shear.

2.2 Key ingredients for severe convective gusts

Many studies, including multiple in-depth textbook on mesoscale atmospheric physics, discuss the most important ingredients for strong and long-lived deep moist convection. These include instability, strong wind shear and a lifting mechanism. However, few studies have specifically looked at convective environments that support damaging wind gusts, with the study of Kuchera and Parker (2006) as an exception. They used 7000 documented severe convective winds events since 2003 in the United States and compared them with the RCM Rapid Update Cycle (RUC, horizontal resolution 20 km) to test the ambient conditions associated with these storms. In addition, they looked at cases where strong convection did occur, but were not paired with widespread damaging winds. In general they found that atmospheric patterns belonging to strong convective situations with severe convective gusts ($\geq$ 25 m/s) are closely related to instability and a combination of wind direction and shear. These two key ingredients are discussed in the next two sections.

2.2.1 Effect of latent instability and CAPE

The initiation of deep moist convection requires that an air parcel reaches a level where it becomes warmer than the environmental temperature (level of free convection; LFC) and stays positively buoyant during its upward journey. A commonly used measure for an air parcel's ability to do so is convective available potential energy (CAPE; Moncrieff and Miller, 1976). CAPE is defined as:

$$\mathrm{CAPE} = \int_{\mathrm{LFC}}^{\mathrm{EL}} B \, \mathrm{d}z \approx g \int_{\mathrm{LFC}}^{\mathrm{EL}} \frac{T_v'}{T_v} \, \mathrm{d}z \tag{2.1}$$

Where EL is the equilibrium level, or the height at which a buoyantly lifted air parcel becomes neutrally buoyant. Otherwise said, the altitude at which the parcel's temperature is the same as the environmental temperature. The B represents buoyancy, g the gravitational constant, T_v' the virtual temperature perturbation of the air parcel compared to the environment and T_v the virtual temperature of the parcel itself. A higher CAPE value indicates a higher potential for kinetic energy gain from the environment as a result of buoyant forces to the vertical acceleration, and ensures that initiated convective updraft can become strong.

The magnitude of CAPE is not directly related to the severity of the convective event, though the studies by Groenemeijer and Van Delden (2007) and Cohen et al. (2007) indicate that for the Netherlands and the US, respectively, instability measured by CAPE has considerable skill in distinguishing weak from severe convective systems. Kirkpatrick et al. (2011) studied 225 numerical simulations of convective storms to examine their behaviour in environments with varying CAPE values. They found that at CAPE values less than 450 J/kg it is very unlikely to generate severe storms, though one supercell storm was found. CAPE values below this threshold indicate that the buoyancy of the rising air parcels is not strong enough to reach great heights, and deep convection is absent. Instead, convection is contained to shallow levels, which rarely results in extreme weather. At a CAPE of 800 J/kg mature storms are more common and updrafts correlate with robust low-level lapse rates. At 2000 J/kg and higher, updrafts benefit from increased shear and higher altitudes of free convection (Kirkpatrick et al., 2011). The relation of CAPE with convective storm development has been studied for decades, i.e. Weisman and Klemp (1982) also confirmed that as CAPE increases from 1000 to 2000 J/kg, storm updraft velocity increases. The study of Kuchera and Parker (2006) specifically into severe gust environments also reports that CAPE is one of the most skill full parameters in predicting gust severity convective situations.

Some studies use the lifted index (LI) as a measure for latent instability. As an alternative to CAPE, LI is defined as the temperature difference of the ambient air at 500 hPa and of an air parcel lifted adiabatically from the surface to that altitude (Galway, 1956). A negative LI value indicates positive parcel buoyancy and subsequently latent instability at 500 hPa (Normand, 1938). For $0 > \mathrm{LI} \geq -2$ the situation is considered slightly unstable, for $-2 > \mathrm{LI} \geq -6$ unstable, and for $\mathrm{LI} < -6$ very unstable.

An environmentally high CAPE alone is not sufficient for convective initiation. This is due to the existence of convection inhibition (CIN) in the atmosphere. The definition of CIN is similar to CAPE:

$$\mathrm{CIN} = \int_{\mathrm{SFC}}^{\mathrm{LFC}} B \, \mathrm{d}z \approx g \int_{\mathrm{SFC}}^{\mathrm{LFC}} \frac{T_v'}{T_v} \, \mathrm{d}z \tag{2.2}$$

Note that the integration of buoyancy now extends from the surface level (SFC) to LFC, instead of from LFC to EL for CAPE. Convective inhibition is usually the result of a capping stable layer or inversion. For air parcels to overcome CIN and to initiate deep moist convection, a lifting mechanism is required. This often is provided by air mass fronts, including outflow boundaries and sea breezes, synoptic fronts, convective cold pools in addition to orography (i.e. Doswell III, 1987; Johns and Doswell, 1992). Kuchera and Parker (2006) found that although a reduction of CIN is a necessity for the initiation of convection, once organized convection is developed, CIN does not substantially impede the generation of strong surface winds.

Note that both CAPE and CIN are dependent on T_v, which in turn is inherently dependent on the presence of water vapor in the atmosphere through the effect of moisture on density. When an air parcel rises it is adiabatically cooled. If the temperature of the parcel drops below the critical temperature for condensation, phase changes might occur, which in turn leads to latent heat release. This enhances convection, as the air parcel gains extra buoyancy in this process to ascend to a higher level.

2.2.2   Effect of wind shear

Several studies indicate that the presence of wind shear strongly affects the organization, development and propagation of severe convective storms (for example, Weisman and Klemp, 1982; Markowski and Richardson, 2011). Vertical wind shear tends to increase the duration and promotes organisation of the storm, though excessive shear is potentially destructive for weak updrafts in situations with little instability (Markowski and Richardson, 2011). One commonly used measure for vertical wind shear is the vector difference between the surface to 6 km wind (often named 0-6 km shear), though alternative levels are also used for the computation of shear. For example, Bechtold and Bidlot (2009) instead use shallow shear (between 850 hPa and 950 hPa wind speeds) to estimate gusts in extreme conditions. Section 2.1.5 on tornadoes and the discussion of the study of Thompson et al. (2003) indicate that shallow shear might be a better discriminator for distinguishing tornadic from non-tornadic supercells. More commonly however, including in the textbooks of Lin (2007) and Markowski and Richardson (2011), the 0-6 km shear is used for separating severe from non-severe environments, and this convention will be adopted in this study.

The 0-6 km shear magnitudes are classified as:

- weak shear: $\leq$ 10 m/s.

- moderate shear: 10-20 m/s

- strong shear: $\geq$ 20 m/s

There are two main theories that explain why vertical shear tends to increase the longevity, organization, and severity of convective storms. First, as vertical shear over the updraft depth strengthens, the outflow and precipitation of the downdraft interfere less with the updraft. This is because the horizontal movement of air influences the position where the downdraft reaches the surface relative to the updraft. Without shear, there the outflow tends to undercut the updraft (see for example Figure 2.1c, versus 2.3). Second, vertical shear has an enhancing effect due to the possible genesis of vertical pressure gradients. This pressure gradient in turn facilitates the lifting along a gust front, and the development of new convective cells (Markowski and Richardson, 2011).

As a rule of thumb from Markowski and Richardson (2011), gust fronts are able to initiate new cells repeatedly at a vertical wind shear between 0 to 6 km of around 10 m/s. Below this, the gust front of single-cells are unable to initiate new cells. With shear between 10 to 20 m/s,

the system reproduction is dominated by gust-front lifting, allowing for the existence of multicell storms. Above around 20 m/s, updrafts can be steady and propagation of the system is regulated by vertical pressure gradients, as opposed to only by gust-front lifting (Markowski and Richardson, 2011).

In addition to the shear magnitude, Kuchera and Parker (2006) found that the ground-relative velocities have good skill in predicting gust damage occurrences. This is the case when warm wind blows over a cold air mass such that convection is detached from the surface, and damaging wind occurrence is diminished. Another case is when wind blows parallel to the convective gust front. In such situation, the convective system produces less severe gusts, as the descending gusts and system speed cancel each other to some extent.

2.3 Projections of environmental conditions for severe convective storms

Summarizing the previous sections, the main atmospheric favorable conditions for the development of severe convective storms are latent instability, a lifting mechanism to overcome convective inhibition and deep-layer wind shear. If the key ingredients for convective storms are projected to change in a warmer climate, it is likely that the characteristics and/or frequency of extreme convective gusts themselves will do so too. Indeed, apart from global temperature increases, climate change is thought to evoke a number changes in the troposphere. These alternations include widespread higher water vapor contents in the lowest layers of the atmosphere, as well as both locally increasing and decreasing mid-tropospheric humidity. In addition, studies suggest that as a result of polar amplification, the process describing the phenomenon where the Arctic regions are warming quicker than lower latitudes, that the polar jet stream has started to meander. This has potential consequences for vertical wind shear in Europe (Petoukhov et al., 2016; Coumou et al., 2018). Amplified low-level humidity increase convective instability and consequently updraft strength. In contrast, decreased mid-tropospheric water contents suppresses convective storm genesis. In this section three studies into the changes of thunderstorm environments in Europe (Rädler et al., 2019; Púčik et al., 2017) and the United States (Diffenbaugh et al., 2013) are discussed in more detail.

One of the more recent investigations for Europe was done by Rädler et al. (2019). They used an ensemble of 14 RCM simulations of the EURO-CORDEX initiative (Jacob et al., 2014) to study the probability of severe convective weather events at the end of the 21st century in Europe, in the RCP4.5 and RCP8.5 carbon emission scenarios (Stocker et al., 2013, see section 3.1.2). The used simulations have a horizontal resolution 50 km, at a 6 hour temporal resolution. As the desired convective hazards addressed are too short-lived and local to be resolved at this resolution, they developed a collection of statistical models to depict these small-scale hazards (Rädler et al., 2018). In these statistical schemes parameters representing mid-level water content, instability and deep-layer shear are used as predictors for convective hazards. The parameters were fitted to observations of lightning, wind and hail (Rädler et al., 2019). Their results suggest that the frequency of extreme convective weather phenomena, including hail, severe gusts and lightning, increases by the end of the 21st century, for most of Europe, except southwestern and southeastern regions. The main explanation provided is increased convective instability as a consequence of higher humidity close to the surface. Furthermore, it is argued that even though polar amplification can lead to weakened jet streams and consequently vertical wind shear, the changes in the stream are minimal and can actually increase in situations with convective instability (Rädler et al., 2019).

A second study exploring the occurrence of favorable environmental conditions for extreme convective storms using the same data as Rädler et al. (2019) in Europe was performed by Púčik et al.

(2017). These conditions include the joint presence of strong deep-layer (surface to 500 hPa) shear and increased latent instability. They report that the model ensembles from the EURO-CORDEX simulations indicate a robust increase in the prevalence of unstable environments (LI ≤ -2) across south and central Europe by the end of the 21$^{\text{st}}$ century, coinciding with increases in the lower-tropospheric moisture. Changes in occurrence of strong (≥ 15 m/s) deep-layer shear are projected to be minimal and not robust except for some areas in northern Europe, where a decline is reported. However, the frequency of situations where latent instability is high and comes paired with strong vertical deep-layer shear is expected to increase by up to 100% in the RCP8.5 scenario in central and eastern Europe (Púčik et al., 2017). The ensemble showed an increase in all models, though a variation in relative change of the frequency of severe environments persists between 25 to 100%. One of the models of the EURO-CORDEX ensemble is RACMO forced with EC-Earth with a reported frequency change of 60% between 1971-2000 to 2071-2100 in the RCP8.5 scenario. The amount of strongly sheared events is not projected to increase, and the robust change mainly comes from an increase of unstable events. The spatial variation of the increased occurrence of severe environments is shown in Figure 2.6.

A third study was performed by Diffenbaugh et al. (2013) who studied potential rises in the frequency of severe thunderstorm environments in the United States using a GCM ensemble. They found a robust rise in the amount of days where high CAPE is combined with strong wind shear. Even though the mean shear is projected to drop, these decreases are concentrated in days with low CAPE and therefore do not lower the number of severe convective environments. In addition, they found that the shift towards higher CAPE is most concentrated in days with low convective inhibition.

To summarize, the studies discussed in this section project that the frequency of favorable conditions for severe storms increases in Europe and the United States by the end of the 21$^{\text{st}}$ century. The resolution of the GCM and RCM ensembles used are, however, too coarse to resolve convective storms and gusts explicitly, and therefore the extent to which this potential for extreme weather is used and relating the predictors to hazard probability remains unaddressed. To this end, convection permitting RCMs can give a way out and will be used in this thesis. Methods to represent convection and associated gusts in CP-RCMs are discussed in the next section.

Frequency of convective severe environments
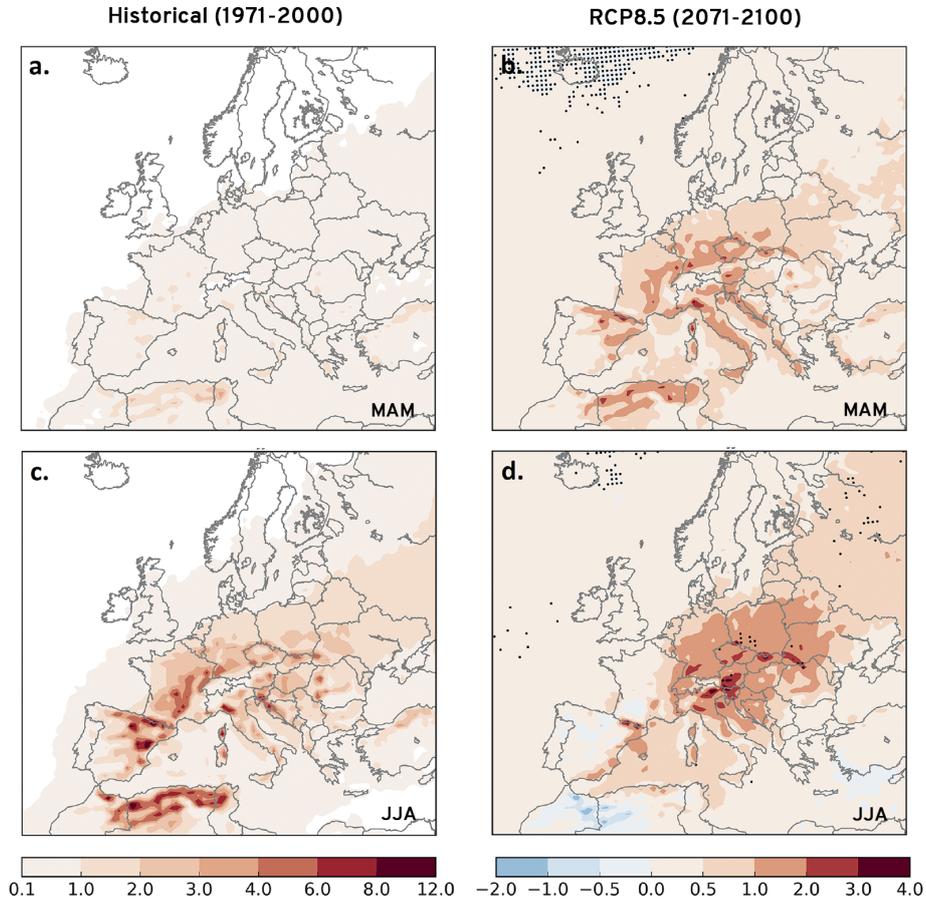
Figure 2.6: *The left two figures show the mean yearly count of convective severe environments in history (1971-2000) in (a) spring (MAM) and in (c) summer (JJA). The right two figures show the change in the mean annual number of severe environments between the RCP8.5 (in 2071-2100) and history in (b) spring and (d) summer. Figure adapted from Púčik et al. (2017).*

.

2.4 Representation of convection in RCMs, parameterization schemes and model resolution

The local and short-lived nature of convective storms raises the question whether they can be resolved in the coarse resolutions of many GCMs and RCMs with horizontal resolutions larger than 10 km. In any model, features smaller than the grid size cannot be resolved explicitly and need to be translated to resolvable scales of motion. This is approach is named parameterization (Anthes, 1985). Due to computational advances, an increasing amount of regional climate simulations are downscaled to convection permitting (CP) scales. In CP models, the horizontal grid size is below 4 km allowing them to explicitly resolve deep convection. Note that at this resolution, shallow

convection and wind gusts are still parameterized. Shallow convective situations rarely result in severe weather (Markowski and Richardson, 2011), and further discussion of these parameterization schemes is therefore left out for brevity. For a schematic overview of model resolution compared to the phenomena studied, see Figure 2.7.
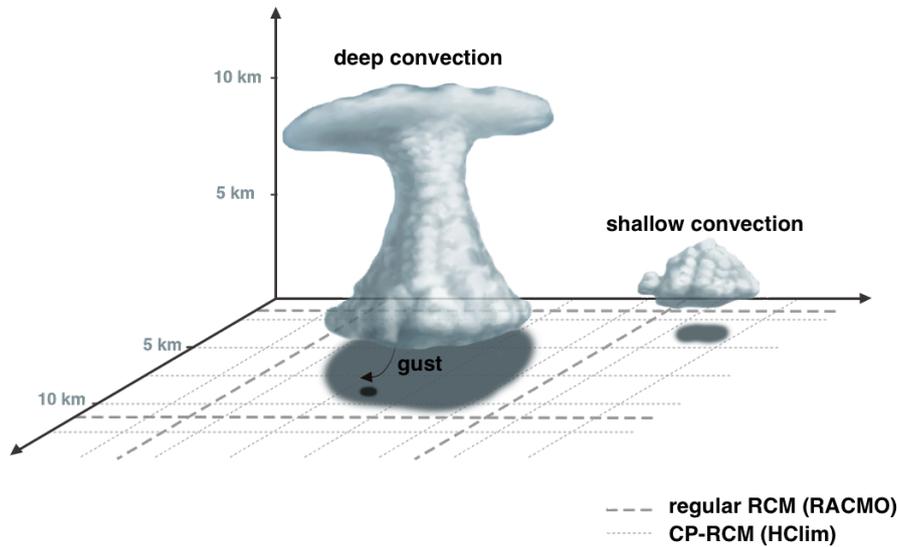
Figure 2.7: *The grid sizes of convection permitting RCMs (in this case, the 2.5 km grid of HClim) and regular RCMs (in this case, 10 km of RACMO). In a classic model, deep convection is smaller than the grid size and needs to be parameterized, whereas they can be explicitly resolved in CP-RCMs. Independent of grid size, shallow convection and wind gusts still need to be parameterized, as they are of smaller scale (motion) than the model's resolution.*

The CP-models are no longer reliant on deep convection parameterization schemes that have been long identified as a significant source of uncertainty and errors (i.e. Déqué, 2007). Another advantage is that CP-RCMs follow the orography and surface fields more accurately.

The work of Prein et al. (2015) provides a solid overview of the potential and challenges of modelling at convection permitting scales. They mention that the largest added value of CP-RCMs over larger scale models can be found on phenomena that occur on small temporal and spatial scales (subdaily and $\leq$ 100 km), processes related to deep-convection, extreme situations, and in complex terrain (such as coast lines, lakes and mountainous areas). As convective storms are related to at least these first three, it can be concluded that CP-RCMs provide a promising tool for upcoming climate research related to extreme convective storms. In fact, the benefits of using CP over regular RCM models is extensively discussed in literature for extreme precipitation. To the best of our knowledge, however, there has not been a specific study on the use of CP-RCMs and benefits for extreme convective gusts. Possibly, the benefits of using CP-RCMs for extreme convective gusts are similar to those for extreme precipitation.

For extreme precipitation there is general scientific agreement on the added value of using CP-RCMs over coarser models: CP-RCMs are better able to reproduce the intensity, frequency, and

location of extreme rainfall. Two examples, one for the United states and one for Europe, are briefly discussed.

Kendon et al. (2017) studied the advantage of convection permitting modelling for climate change research at mid-latitudes in Europe. Their study reports that explicit representation of convective storms is essential for studying alternations in intensity and duration of summertime rain. They also mention that convection-permitting resolutions are required to capture changes in convective severe wind gusts, as severe convective squall lines can only be represented on convection-permitting scales (Kendon et al., 2017). Though their statement makes logical sense, it is not supported by any scientific data.

Prein et al. (2017) show that simulations using a 4 km convection permitting model in the United States in summer are able to capture the key features of mesoscale convection events, such as their size, precipitation rate, lifetime and propagation speed. However, the frequency of the convective storms in central US regions is significantly underestimated. A similar frequency bias was found by Liu et al. (2006). Both studies suggest that the discrepancy in frequency is mainly in periods of weak synoptic forcing.

Systematic deficiencies remain in CP simulations, especially in the representation of the diurnal cycle of convection (Baldauf et al., 2011; Prein et al., 2015). In addition, sensitivities are reported with regard to convective cell sizes, intensities and initiation times to the mixing-length parameter in the subgrid turbulence schemes (Hanley et al., 2015). Likely, a significant part of the deficiencies are related to inaccurate representation of the initiation of convection and planetary boundary layer processes (Baldauf et al., 2011; Hirt and Craig, 2020), especially related to convective initiation related to cold pools. The explosion of the use of models at convection permitting scales for climate study stimulates the ongoing effort to improve the dynamics of convection permitting models.

2.4.1 Gust parameterization schemes

As visualized in Figure 2.7, the eddies responsible for wind gusts are of subgrid scale and their effects need to be related to resolvable scales of motion through parameterization. Generally, two groups of gust parameterisations are defined. In the first group, the methods are based based on the reasoning that gusts and atmospheric turbulence (and hence turbulent kinetic energy; TKE) are related. The methods in the second group are based on the assumption that gusts result from air particle deflection from higher altitudes. Moreover, some models specify different techniques for forecasting gusts in convective and non-convective situations. The report of Sheridan (2011) provides a good overview of the techniques used for both convective and non-convective gust parameterization, and which models at the time used which schemes. In general, gust parameterization schemes can be divided into four categories, see Figure 2.8 for a summary.

In the first category, parameterizations are based on the relationship of near-surface winds to the friction velocity u_* after Panofsky et al. (1977). Methods in the second category use the tactic of checking upwards, to the first stable layer, the boundary layer top, or another chosen level, to identify heights from which momentum may be transported downwards. Here, the argument is used that there is no barrier imposed to downward mixing of momentum below these heights. With this assumption, the scheme uses an algorithm that searches for the maximum wind encountered in these heights. The third group is based on the theory that gusts are directly indicative of the amount of turbulence in the boundary layer. In this category, the gust strength is related to the turbulent kinetic intensity. In some cases, the boundary layer stability is additionally taken into account by assuming that turbulence depends on atmospheric instability (Schreur and Geertsema, 2008). In the fourth category the methods are based on the wind gust estimate of Brasseur (2001). This scheme has similarities with methods in the second category. In this case however, the levels

from which momentum can be transferred to the surface are selected more delinquently. Namely, the level in which the maximum wind speed is searched must have a sufficient TKE to overcome possible buoyant inhibition. In this manner, the scheme in addition has common grounds with the TKE method of the third group.
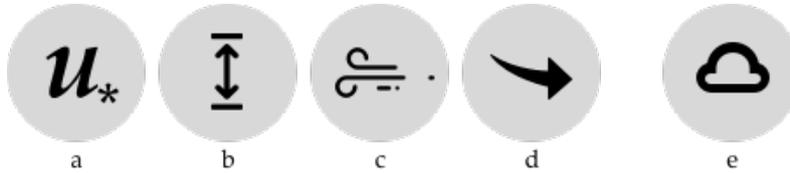

Figure 2.8: *In general, RCM gust parameterization schemes can be divided into four groups. The first group (a) uses the relationship of near-surface wind to friction velocity, the second group (b) uses the maximum wind speed within a particular set of atmospheric levels, the third (c) is based on TKE and the fourth (d) on downward transport of vertical momentum. See the text for a more detailed discussion. In addition, some models use a separate scheme (e) for convective situations.*

Some models use an alternative or additional parameterization scheme in case of convective situations. These schemes are based on vertical momentum equations and basic concepts of air motion within convective cells, see Prein et al. (2015) for a brief overview.

In multiple studies the performance of various gust parameterization schemes in RCMs is addressed. For example, Kurbatova et al. (2018) assess the performance of various schemes from all four parameterization categories (Figure 2.8) and combinations thereof for the Russian part of Europe. In this study, a hybrid model is also proposed: using TKE parameterisation when the Richardson number is high, and the method of Brasseur (2001) where the energy of particles reaching the surface is taken into account. None of the studied schemes, including the combined algorithms, come out as the best method, and the report shows the need for further research into the methods for representing gusts in RCMs.

A second study into the performance of various parameterization schemes was done by Minola et al. (2020). They improved the mean and wind gust discrepancy between observations and model for ERA5 (Hersbach et al., 2020) across Sweden. ERA5 is a global reanalysis product with a horizontal resolution of approximately 30 km. The gust parameterization in ERA5 is similar to RACMO (see section 3.1.4) where gusts are the sum of the instantaneous wind, and the turbulent and convective contribution to gustiness. The results of Minola et al. (2020) show that the contribution of the convective term is minor (below 0.5 m/s) when looking at the mean seasonal cycle across a region in Sweden, and that the expected seasonal cycle with a higher convective contribution in summer is absent. Following this, tuning procedures were tested to improve the formulations of the convective contribution to the total gustiness. First, an elevation-dependent coefficient is incorporated in the turbulent contribution. Second, the convective mixing parameter was tuned. The tuning methods and a combination thereof led to a modest improvements of the parameterization of the wind gusts, especially over mountainous regions, for all hourly, daily, daily max and monthly gusts.

Both the investigations of Kurbatova et al. (2018) and Minola et al. (2020) into improving model performance for gusts by looking at various gust parameterization schemes were applied to relatively coarse resolution models. To the best of our knowledge, no formal study so far has looked at the performance of various gust parameterization schemes in relation to the model resolution, let alone separately for convective gusts.

The models used for this study are more extensively discussed in chapter 3. To put the discussion of the gust parameterization in better context to this report, the next two sections describe the

parameterization schemes of the two RCMs used in this study: Harmonie Climate (HClim) and RACMO, section 3.1.4 and 3.1.5.

2.4.2 Gust parameterization in RACMO

In the RACMO model, gusts are computed in multiple steps (ECMWF, 2009). These steps are first undertaken for the separate wind directions, with U_{gust} representing the east-west component and V_{gust} in north-south component. In the following steps the process is only shown for U_{gust}, though the same method applies for V_{gust}.

To start, the standard deviation of the horizontal wind, σ_U, is computed based on the similarity relation of Panofsky et al. (1977):

$$\sigma_U = 2.29u_* \left(1 - \frac{0.5}{12}\frac{z_i}{L}\right)^{1/3} \qquad \text{for } L < 0 \qquad (2.3)$$

$$\sigma_U = 2.29u_* \qquad \text{for } L \geq 0 \qquad (2.4)$$

Where u_* is the friction velocity, L is the Monin-Obukhov length and z_i is 1000 m (ECMWF, 2009). Next, the gust speed is computed with the wind speed at 10 m, U_{10m}, plus a factor proportional to σ_U. Consequently, the computation of the wind gust looks as follows:

$$U_{gust} = U_{10m} + 7.71u_* \qquad (2.5)$$

The number 7.71 is based on the work of Beljaars (1987), who studied universal turbulence spectra. From equation 2.5 it is visible that the effects of both surface friction, through u_*, and stability, through L, are taken into account. In situations of baroclinicity or gusts originated from strong convective events, this approach is not adequate. Therefore, in cases when deep convection is active, an extra contribution is added. This contribution is a function of the vertical wind shear added to equation, after the work of Bechtold and Bidlot (2009):

$$U_{gust,conv} = U_{10m} + 7.71u_* + C_{\text{conv}} \max(0, \ U_{850} - U_{950}) \qquad (2.6)$$

Where $C_{\text{conv}} = 0.6$ represents the convective mixing parameter, and $U_{850} - U_{950}$ the difference in wind speed between 850 and 950 hPa. The gust speed in both directions is computed at every model time step, and the maximum value of $\sqrt{U_{gust}^2 + V_{gust}^2}$ since the last post-processing interval is saved as output (ECMWF, 2009). For this study, gust data from RACMO alone are available at 3 hour intervals for the entire 21$^{\text{st}}$ century.

2.4.3 Gust parameterization in Harmonie Climate

At a resolution of 2.5 km, HClim is able to resolve deep deep convection roughly resolved and represented in the model's non-hydrostatic dynamics. In contrast, shallow convection is still parameterized. In HClim gusts are parameterized as (Amodei et al., 2015 and Tijm, 2020: pers. comm.):

$$U_{gust} = U_{10m} + 3.5 * \sqrt{TKE} \qquad (2.7)$$

Where TKE is the turbulent kinetic energy and U_{10m} the average wind speed at 10 m. For every model time step U_{gust} and V_{gust} are kept temporally and when $\sqrt{U_{gust}^2 + V_{gust}^2}$ is maximum, U_{gust} and V_{gust} is output hourly.

2.4.4 Comparing the RACMO and Harmonie Climate parameterizations

In short, the parameterization schemes of RACMO and HClim consist of the sum of the instantaneous wind and total gustiness. In HClim, the total gustiness is purely based on TKE and falls into the third parameterization category (Figure 2.8c). The RACMO parameterization belongs to the first category (Figure 2.8a), with an addition for convective gustiness (2.8e). Note that both schemes are roughly equal with respect to their first term near the surface.

However, this term is primarily based on TKE, and argued to be only applicable to strong convective situations when the turbulence is of mechanical origin (Kurbatova et al., 2018). In RACMO, gustiness is determined as the sum of turbulent and convective gustiness, where the former in its turn is based on the shear stress as a function of friction velocity, and the latter is proportional to the low-level wind shear between 950 and 850 hPa, and a tunable convective mixing parameter.

In contrast in HClim, there is no added term in case of deep convection. Possibly, this is not necessary anymore as deep convection is explicitly resolved in the CP-RCM. In this case, extra TKE is added automatically when air is disturbed by cold, convective outflows over warm surfaces. However, the net effect on the performance of convective gust modelling of not adding a term when deep convection is active, but increasing the resolution to convection-permitting scales, needs to be addressed in future research.

Chapter 3

Data, Models and Simulations

The data used for this thesis are extensively discussed in this chapter, and the methodology is addressed in more detail in chapter 4. Data processing is entirely done with Python and in the command line through Climate Data Operators; the codes are available on request.

3.1 Modelled data

General circulation models (GCMs) and non-convection permitting regional climate models (RCMs) can provide background information into climate change processes. Their resolutions are usually insufficient to resolve the complex dynamics of small-scale convective systems and therefore use parameterization schemes for convection (see chapter 2). Such simplified schemes are likely not reliable when studying the effects of climate change (Kendon et al., 2017). Consequently, GCMs and RCMs are often downscaled using convection-permitting (CP) models. For a broader discussion on the use of convection-permitting models to investigate climate change effects on gust see section 2.4. The GCM, RCM and CP-RCM output used for this study come from EC-Earth, RACMO and Harmonie Climate (HClim), respectively. In addition, to assess the performance of HClim, we use a run that is forced with the global atmospheric reanalysis product ERA-interim. The relation between the RCMs and forcing data sets is visualized in Figure 3.1, and the models are discussed in more detail in the next sections.

3.1.1 General circulation model EC-Earth

In this study the effects of climate change are assessed using an ensemble of 21st century climate projections with the GCM EC-Earth (Hazeleger et al., 2012). The model consists of an atmospheric component from the Integrated Forecast System (IFS) of the ECMWF and an ocean component Nucleus for European Modelling of the Ocean (NEMO). For Europe, EC-Earth has a horizontal resolution of approximately $1°$ or 125 km. The EC-Earth simulations for the 21st century are forced with higher atmospheric carbon concentrations as based on the RCP8.5 scenario, that is discussed in the next section.

3.1.2 Climate scenario RCP8.5

In the lead-up to the Fifth Assessment Report (AR5) authored by the International Panel on Climate Change (IPCC), scientists developed four scenarios of greenhouse-gas emissions by the end of the
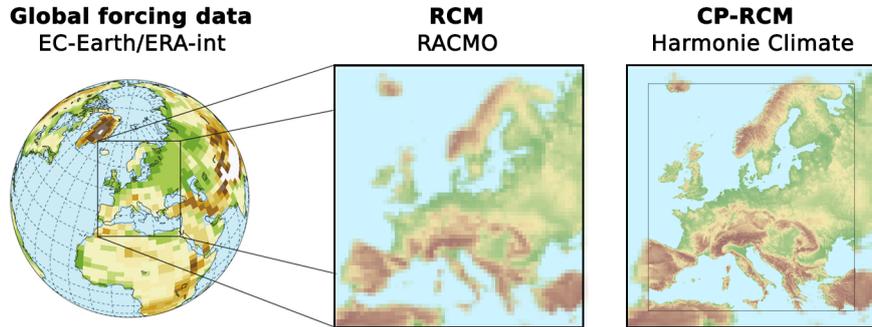
Figure 3.1: *The relationship between ERA, EC-Earth, RACMO and HClim visualized schematically. The GCM and reanalysis data set are regionally downscaled by the non-convection permitting RCM RACMO, which in turn is used for boundary conditions for the CP-RCM HClim. The pixelation is for illustrative purposes and does not represent the actual resolution of around 50, 10 and 2.5 km for EC-Earth and ERA, RACMO, and HClim, respectively (own illustration).*

21st century, known as the Representative Concentration Pathways (RCPs) (Stocker et al., 2013). The mildest of four scenarios portrays a world were global temperature increases remain below 2°C with respect to pre-industrial temperatures. The most extreme scenario, RCP8.5, sketches a dystopian future when fossil fuel usage increases and no mitigation measures are taken. The number 8.5 indicates the expected radiative forcing by greenhouse gasses of 8.5 W/m^2 in 2100, equivalent to an atmospheric CO_2 concentration of 1200 ppm. The report projects a global temperature increase for this scenario of 3.7°C between 2081-2100 relative to 1986-2005, with a likely range between 2.6° to 4.8°C (Stocker et al., 2013). Some scientist argue this to be a likely pathway, especially for the mid century analyses (Schreur and Geertsema, 2008). On the other hand, some argue that the RCP8.5 scenario is becoming increasingly implausible for the end of the century (Ho et al., 2019; Hausfather and Peters, 2020). They mention that in order to follow the RCP8.5 scenario, an unmatched fivefold increase in coal use by 2100 is assumed. However, some argue that this amount is larger than some estimates of global coal reserves (Ritchie and Dowlatabadi, 2017). Besides, many energy forecasts expect the coal use to reach a steady-state in the near future, and the falling costs of renewable energy is unlikely to reverse (IEA, 2019).

3.1.3   Global reanalysis data set ERA-interim

The performance of the EC-Earth forced runs is validated using the global atmospheric reanalysis product ERA-interim. This data set is formed from a combination of the weather forecasting model of the European Centre for Medium-Range Weather Forecasts (ECMWF) and observations (Dee et al., 2011). In a global atmospheric reanalysis data set, the combination of archived observations assimilated with forecast models allows for consistent convenient maps without gaps of global historical weather as close to reality as possible. The ERA-interim data set is available between 1979 and 2019 at a resolution of roughly 80 km on 60 vertical levels up until 0.1 hPa (Dee et al., 2011).

3.1.4 The RACMO model

The GCM and reanalysis set are applied to the lateral boundaries of the RCMs, first to the coarser RCM RACMO2, which in its turn provides boundary conditions for the CP-RCM HClim, see Figure 3.1. RACMO2 is a hydrostatic model and operates at a resolution of roughly 12 km (Van Meijgaard et al., 2012), and is from now on referred to as RACMO. The lateral boundary conditions for the RCM run are taken from the global forcing sets as discussed before, but away from the boundaries the RCM is free to evolve according to its own physics. The RACMO extent is from $-25.3°$ to $27.8°$ east and $39.5°$ to $65°$ north. Note that the RACMO domain is cropped in the southern domain in post-processing; the RACMO domain therefore extends less to the south than the HClim domain in the figures depicted in this report. The physics of RACMO are based on the physics of the HIRLAM semi-Lagrangian dynamics version 5.0.6. More details about the physical processes embedded in RACMO can be found in ECMWF (2009). Cumulus convection is parameterized according to the bulk mass flux scheme, that was originally outlined by Tiedtke (1989). In addition to providing boundary conditions for the CP-RCM, RACMO data are also studied directly without the downscaling of HClim.

3.1.5 Harmonie Climate

The CP-RCM data used for this study comes from the non-hydrostatic and convection permitting regional climate model HCLIM-AROME (cycle 38) (Belušić et al. (2020), from now on Harmonie Climate or HClim). HClim is a collaboration between ALADIN and HIRLAM consortiums in Europe (Bengtsson et al., 2017). The model is based on the physics and non-hydrostatic dynamics of AROME (Seity et al., 2011) and includes adjustments in the physics developed by the Hirlam community (Bengtsson et al., 2017). At a resolution of 2.5 km, deep convection is roughly resolved and represented in the model's non-hydrostatic dynamics, whereas shallow convection is still parameterized. The physics shallow convection parameterization is derived from the eddy diffusivity mass-flux scheme (De Rooy and Siebesma, 2008; Bengtsson et al., 2017).

The works of Tijm (2018) and Veen (2019) show a severe underestimation in the amount of modelled shallow showers in Harmonie at a resolution of 2.5 km. They relate this bias to a too active shallow convection scheme. In an attempt to improve the model, Veen (2019) shows that increasing the model's horizontal resolution does not improve the bias. It is suggested that the biggest gains can be found in the improvement of the microphysics scheme.

The experiment used for this study is centered over central western Europe, between $-12.8°$ and $18.8°$ east and $37.0°$ and $58.5°$ north. The HClim variables are available at 1 and 3-hourly intervals. The instantaneous values presented in this thesis at rounded hours (1 pm , 2 pm etc). Fluxes are computed from the hourly difference of the cumulative fields, and are therefore average fluxes of the hour stored every mid hour (1:30 pm etc.). Gusts are written as the maximum over the hour and are also stored every mid hour.

The CP-RCM runs of HClim come with high computational costs. Therefore, RACMO forced with EC-Earth is not downscaled for the entire 21st century but instead at three distinct time periods of 10 years. The first and historical run covers a time span between 1996-2005 (historical; hist). The second spans the mid of the 21st century (mid of century; MOC) between 2041-2050, and the third addresses the end of the 21st century (end of century; EOC). The ERA-interim forced RACMO is downscaled through HClim between 2000-2009. An overview of the model runs used for this study is summarized in Table 3.1.

Acronym	Model	Forcing	Resolution	Time span
HClim-ERA	HClim	ERA-interim, RACMO	2.5 km	2000-2009
HClim-hist	HClim	EC-Earth, RACMO	2.5 km	1996-2005
HClim-MOC	HClim	EC-Earth, RACMO	2.5 km	2041-2050
HClim-EOC	HClim	EC-Earth, RACMO	2.5 km	2090-2099
RACMO-hist	RACMO	EC-Earth	10 km	1996-2005
RACMO-EOC	RACMO	EC-Earth	10 km	2090-2099

Table 3.1: *Modelled data sets available for this study. Note that the temporal resolution of the Harmonie Climate (HClim) runs depends on the output variable and ranges between 1-hourly output to daily output, and for RACMO all variables are available as 3-hourly output. Even though the HClim sets span 11 years of data, the first year is used as a spin-up year and not used in the data analysis. The RACMO data are available for the entire 21st century, but only the years overlapping with HClim-hist and HClim-EOC are used. One HClim grid cell covers an area of approximately 2.5×2.5 km^2, one RACMO cell roughly 10×10 km^2.*

3.2 Observational data

To assess the ability of Harmonie Climate to capture convective storms, observational data from the Royal Netherlands Meteorological Institute (KNMI) are used. KNMI has a network of 50 operational observation stations from which data are readily available at hourly intervals. Figure 3.2 shows the location of these stations. Note that the density of stations is higher near the coast than further inland. The observational data are taken in the same period as the HClim-ERA forced run (2000-2009), but some stations have significant missing data ($\geq 5\%$ of hourly data missing) in the desired time period. These are left out of this study, leaving us with 34 stations for the performance assessment of the models.

Wind climatology strongly depends on the geography and terrain characteristics of a region (for example, Jiménez and Dudhia, 2012). As a start, stations can be divided into inland and coastal stations as the physical processes that influence the wind climatology differs for these groups. The climatology of coastal stations is ruled by variations between land and sea, such as sea breezes, and step-like changes due to sudden changes in surface roughness and surface temperature. Inland stations are highly dependent on land-atmosphere interactions and land surface processes. To make sure that the nearest grid cell of the HClim and RACMO models to the stations does not overlap with water bodies, a distance of at least 12 km is chosen for a station to classify as inland. The total number of stations left with sufficient data for this study is 34, of which 22 are inland stations.

To quantify extreme wind conditions it is not sufficient to solely look at the near surface average wind speed. To take abrupt increases in wind and its turbulent signature into account, the World Meteorological Organisation (WMO) proposes to additionally record the close to the ground surface peak or wind gust, defined as the maximum 3 s wind speed (WMO, 1987). Therefore, gust data from the KNMI stations are used to verify modelled gusts. In addition to gusts this study also compares the model's temperature with observational data to validate if the climate is changing in the model according to the expectations of the IPCC. To this end, the following observed variables are used:

Locations of KNMI observation stations

Figure 3.2: *Locations of the KNMI observation stations in the Netherlands. The red stations are defined as inland, as they are at least 12 km away from the coast. The grey stations are not used as they contain too many missing data in the desired time periods (data from KNMI).*

- Near-surface wind gust: the highest 3 s wind speed in last hour with a precision of 1 m/s. The wind is measured at a height of 10 meters. KNMI also provides data at 10 minute intervals at a higher precision, but unfortunately, this data set commences in 2003. As the historical runs for this study encompass the years between 1996 and 2009 only, the data of coarser temporal resolution available for the entire time domain is used.

- Temperature: measured at 1.5 m above the ground, instantaneous value at hourly intervals, at a precision of 0.1°C.

Chapter 4

Methodology

To analyse the projections of gusts in a future warmer climate both climatological and dynamical approaches are used in this thesis. The methods used for both approaches, as well as those for the performance assessment of the model, are discussed in more detail in this chapter.

4.1 Performance assessment

The performance of the models for gusts will be assessed by comparing their output with observational data from the 22 inland KNMI stations discussed in section 3.2. Note that the two historical runs from HClim span different time periods: 1996-2005 for the ERA-interim forced run and 2000-2009 for the EC-Earth forced history run. Both periods are considered to be climatologically the same for gusts in this study. With this assumption, statistics of both historical runs can be compared to the same 2000-2009 observation period. At the 22 observation locations, model data are extracted at the nearest grid point. The data at every point are compared using several statistics that are presented in the overview below.

Statistic	Description
mean	The standard mean of the series: $\text{mean} = \frac{1}{n} \sum_{i=1}^{n} a_i$
max	The maximum value in the series.
p_{95}	The 95th percentile value of the n ordered values in the series, as determined by the nearest-rank method, such that the percentile will always be a member of the original ordered series.
p_{99}	Similar to p_{95}, but then for the 99th percentile.
RL_{10}	The return gust values for a return period of 10 years, discussed extensively in section 4.4.
RL_{50}	Similar to RL_{10}, but then for the 50 year return period.
f_{20}	Number of summer days with gust ≥ 20 m/s in the total time span of the data set.
f_{25}	Similar to f_{20}, but then for the number of days above 25 m/s.

Note that the RACMO variables are available at 3-hourly output. Therefore, it is more challenging to compare the data with the hourly observation data directly. As a solution, the daily maxima for HClim and RACMO and observations are computed first. This is done as we are mainly

interested in extreme values. These numbers are then used for the computation of the previously mentioned statistics to compare the models.

As this thesis focuses on convective extremes, the statistics are only applied to summer month data when the meteorological conditions favor the organization of deep moist convection. For the Netherlands, this is between May to September. In this way, the statistics are more focused on convective summer situations without taking winter storms into account as well.

Each performance statistic is computed for every location, and data sets are compared by computing the Root Mean Squared Error (RMSE) and the Mean Bias Error (MBE). The RMSE is useful to get a general indication of how much the model data differ from the observational data. The MBE provides an indication of the sign of the error. The formulas used to compute the RMSE and MBE are:

$$RMSE = \sqrt{\frac{1}{n} \sum_{i=1}^{n} (m_i - o_i)^2} \tag{4.1}$$

$$MBE = \frac{1}{n} \sum_{i=1}^{n} (m_i - o_i) \tag{4.2}$$

Where n is the number of locations used, o_i the observation statistic at the ith location and m_i the model statistic at the ith location.

4.2 Fuzzy verification

Note that traditional verification methods such as using the RMSE can provide inaccurate uninformative results for high resolution forecasts of small scale phenomena when compared to observations (Ebert, 2008). The convective storms are often of small scale, and can easily be missed by observation stations as well as by a RCM with a high horizontal resolution, at that time and/or space. Using a spatial window to include data surrounding the event relaxes the conditions for exact matches between modelled and observed storms in time, intensity and space. See Figure 4.1 for a schematic representation of the traditional versus the fuzzy verification methods.

Especially in this study, it is challenging to compare the ERA-Interim forced runs with observations, as the forcing is far away from the boundaries and within the box HClim is allowed to develop its own physics. Therefore, when examining the performance of the HClim model through a historical case study, the observed gust values are compared to a larger area surrounding the station.

In studying climatology instead of specific case studies using a fuzzy verification method is still important for extreme statistics as again, by definition, the rare extreme events can be missed at particular stations or grid cells. Therefore, when assessing the model's performance using the statistics introduced at the beginning of this section, the station wise comparison should be taken with caution. Instead, the statistics of the 22 stations are aggregated and discussed in more detail.

To assess future changes of a larger region instead of single grid points data are spatially aggregated over a box (3° to 8° longitude, and 50° to 54° latitude) surrounding the Netherlands. As an additional requirement, data have to be at least 25 km away from the sea and large water bodies, including the sea-attached IJsselmeer and Zeeland lakes. These aggregated data are used to compute
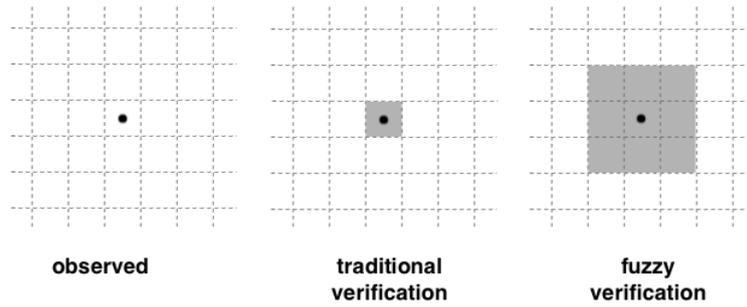
Figure 4.1: *For a particular observation at a station (left), in traditional verification methods modelled results from the same grid box are compared (middle). In fuzzy verification, the neighbourhood surrounding the observation is taken (right). The dotted lines represent the RCM grid size.*

box plots of summer maxima for the various HClim and RACMO model runs. For each day in the 10 years of modelled data, the maximum is calculated and shown in box plots.

4.3 Case studies for end of century analysis

To examine the projected changes of convective storms in the Netherlands from a dynamical perspective, ten case studies are selected from the HClim-EOC, the RACMO-EOC and the HClim-hist run. This is done by selecting land points only (at least 25 km removed from the coast) in summer that have a CAPE value of at least 800 J/kg in a six hour time interval before or after the time of the data point. This instability threshold was chosen after reviewing the study of Kirkpatrick et al. (2011) on the sensitivity of convective storms to environmental CAPE. A more detailed discussion on their findings can be found in section 2.2.1. Next, the remaining data points are sorted from high to low gust values, and the 10 highest values for every model run are kept. The values need to be separated by at least 24 hours to avoid an investigation of the same event.

For the 10 selected maximum events in terms of gusts additional meteorological variables are included in the investigations. Note that for RACMO, all variables are written away every three hours, whereas this varies per variable for HClim, as indicated in Table 4.1. These variables are selected as they are known to come paired with, or as they are conducive for well-organized convective storms. Examples of the latter category are the shear between 500 hPa and the surface (see section 2.2.2) and latent instability as indicated by CAPE (see section 2.2.1). Commonly, the 0-6 km shear is used to predict storm types. As the 6 km wind speed is not available in this study, instead the wind at 500 hPa is used, roughly equivalent to 5.5 km.

Variable	Description	Frequency
Gust speed	The 10 m surface gust speed.	hourly, maximum
Temperature	The 2 m surface air temperature.	hourly, actual
Dew point temp.	The 2 m surface dew point temperature (td2m), calculated using relative humidity and temperature.	hourly, actual
Wind speed	The 10 m wind speed.	hourly, actual
Precipitation	The total precipitation amount in the last hour.	hourly, flux
CAPE	The convective available potential energy.	hourly, actual
Wind shear 500 hPa	The wind shear from surface (10 m) to 500 hPa: where U_{500} and V_{500} are the eastward and northward wind at 500 hPa, respectively, and U_{10m} and V_{10m} the eastward and northward wind at 10 m, respectively. Not available for the RACMO run.	3-hourly, actual
Vert. wind 925 hPa	The vertical wind velocity at 925 hPa. Downwards flows are negative, upwards positive. Not available for the RACMO run.	3-hourly, actual
MSL pressure	The air pressure at sea level.	hourly, actual

Table 4.1: *Overview of variables used for investigation of the case studies in the future runs.*

The case studies from every run are analysed for patterns in the general underlying meteorological conditions. Of these case studies, three are discussed in more detail: two from the HClim-EOC events, and one from the RACMO maximum events. For all days of the case studies an animation of all environmental variables is made, which can be found in Appendix B. The figures shown in this report are from the time when the event is maximum in terms of gust speed. The color scales for the variables are determined by dividing the values into nine bins of equal length from zero to the maximum value rounded to the nearest multiple of five. Three exceptions are made for CAPE, MSL pressure and vertical wind speed. For CAPE, the color scale is capped at 4000 J/kg as very local

and short-lived values of (in some cases up to 7000 J/kg) would otherwise diminish the visibility of variation in other regions. As MSL pressure starts from around 980 hPa, the minimum value of the color bar for this variable was determined by rounding the lowest value to the nearest multiple of five. Vertical wind speeds can have negative magnitudes (indicating downward flow), and the minimum and maximum of the color scales are determined by the absolute value of the variable's maximum on that day, such that the color scale is symmetric. Because of the relatively small magnitude of the vertical wind speed compared to other variables, the maximum and minimum values were simply rounded to the nearest integer, instead of to a nearest multiple of five.

In addition, boxplots of several environmental variables are made to compare the environmental conditions over land of the maximum case studies. To this end, 95th percentiles for various variables that are posed to be key indicators for extreme convective gusts (see Chapter 2.2) are computed over all hours of the event day and coordinates at least 25 km away from the coast (including large water bodies such as the lake IJsselmeer), over all events. These include surface air temperature (tas), surface dew point temperature (td2m), CAPE and shear. In addition, the 95th percentile of the wind speed and the 5th percentile of the MSL pressure (psl), as a measure for the presence of low pressure systems, are computed to get an indication of the general synoptic situation. Also, the maximum value of variables associated with convective storms, such as precipitation, CAPE and vertical wind speeds, are computed over all hours and coordinates of the event day. In the boxplots the environmental conditions of the extreme cases are also compared to the value of the statistic for an average summer day in the model run.

4.4   Extreme value theory

Extreme value analysis is a useful tool for describing the distribution and risk of rare events. Briefly said, two different extreme value analysis methods exist for describing for assessing the asymptotic tail behavior of the studied distribution.

One commonly applied approach is the classical Generalized Extreme Value (GEV) theory. In this method, three distinct distributions are used and only annual maxima values are considered (Fisher and Tippett, 1928; Jenkinson, 1955). The second method is the Peaks Over Threshold (POT) approach. In this method, all events above a carefully selected threshold are kept and a Generalized Pareto distribution (GPD; Palutikof et al., 1999) is fitted to the remaining data. The POT method increases the number of considered events and hence reduces uncertainty when properly applied. The book of Coles (2001) provides a theoretical definition and more detailed explanation of the discussed methods. For this study, the POT method is applied as follows:

1. A certain threshold is chosen. The choice of the threshold is not straightforward, as a higher threshold will result in fewer data left, and hence an increase in variance for the estimators of the GPD fit, and a too low threshold will yield a high bias as it will not satisfy convergence towards the extreme value theory. Many methods have been developed for choosing the right threshold, though interpretation of these methods can be challenging. For simplicity, the threshold for this study is set on the data set's 95th percentile after the recommendations of Caires, 2020 (pers. comm). The data values exceeding this threshold are kept for the next step.

2. The POT method requires the exceedances to be mutually independent. Therefore, the exceeding data are divided into events, such that the events are independent, and the maximum of each event is kept. For this study an event is considered independent if a new data value is at least 24 hours after the previous value above the threshold. Ideally, the gust data should in

addition be split up into different physical categories as various types of events might follow deviating extreme value distributions. One could for example split the data into local, short lived convective events and events that are more related to the synoptic situation. The development of such distinction is time consuming and needs to be done with care, and for brevity not realised in this study besides taking only data from summer (from May to September) months.

3. The excesses above the threshold of the remaining maxima of the independent events are then fitted to a General Pareto Distribution (GPD) given by:

$$G_{\xi,\sigma}(y) = \begin{cases} 1 - \left(1 + \frac{\xi y}{\sigma}\right)^{1/\xi} & \text{if } \xi \neq 0 \\ 1 - \exp\left(-\frac{y}{\sigma}\right) & \text{if } \xi = 0 \end{cases} \tag{4.3}$$

Where ξ is the shape parameter and σ the scale parameter. The parameters are fitted using $\mathcal{L}$-moments (Hosking, 1990).

4. From the found parameters, the return gust values RL can be computed for a desired return period N.

$$\text{RL}_N = t_{\text{p95}} + \frac{\sigma}{\xi}[(\lambda N)^\xi - 1] \tag{4.4}$$

Where t_{p95} is the chosen threshold, σ and ξ are the found GPD parameters and λ is the ratio between the number of exceedances to the number of years of records. In this study return periods of 10 and 50 years were used. The former because 10 years of data is available and will be a more accurate estimate, and 50 years as this is a common metric in wind turbine design, for example Negro et al. (2014). These statistics will be referred to as RL_{10} and RL_{50}.

Chapter 5

Results

5.1 Performance assessment of the historical RCM runs

In this section the ability of HClim and RACMO to model extreme convective gusts accurately is quantified (objective B). The section starts with a general discussion of the gust climatology of the models compared to observations, and is followed by a more detailed analysis on the performance of the models in resolving the frequency of extreme events. The section is concluded with a historical case study of the highest summer gust observed at several inland KNMI stations between 2000 and 2009.

5.1.1 Historical RCM runs gust climatology compared to observations

To assess the performance of HClim and RACMO for convective gusts, model data of the HClim-ERA, HClim-hist and RACMO-hist runs are compared with observations at 22 inland stations in the Netherlands, see Figure 3.2. The result of various statistical comparisons is shown for HClim in Table 5.1 and for daily maxima in RACMO in Table 5.2. See the folder 'Observations vs. Model' in Appendix B for a per station comparison for all models and performance statistics.

The mean and p_{95} values of HClim compare well to observations with MBEs ranging between 0 and 0.1 m/s. For both runs, the only station showing a higher deviation of the mean than 1 m/s is Rotterdam Geulhaven. The observed summer mean gust speed is highest here with 7.9 m/s, whereas HClim-hist and HClim-ERA model 6.8 and 6.6 m/s, respectively. Located in a port, the terrain around the observation tower is complex with canals and industrial terrain next to one another, which might explain the discrepancy. The RACMO-hist mean and p_{95} show a slightly higher deviation from observations with MBEs of 0.8 and 0.6 m/s, respectively. At 20 out of 22 locations the mean daily maximum gust is overestimated in RACMO-hist, and a plausible explanation is given in the next paragraph.

For more extreme statistics, especially for HClim-hist, the performance is worse. The maximum summer gust value in HClim-hist, see also Figure 5.1 for a station wise comparison, is on average 3.5 m/s lower than observed (see Table 5.1). The value is underestimated at 20 of the 22 stations, and for some locations the difference is up to 8 m/s. The performance for the maximum value is much better for HClim-ERA (MBE of -0.7 m/s). This is interesting, as both runs are downscaled with the same CP-RCM and differences cannot be explained by the model itself. The poorer performance of HClim-hist compared to HClim-ERA can possibly originate in a temperature bias in the EC-

		HClim-ERA		HClim-hist	
		RMSE	*MBE*	*RMSE*	*MBE*
mean	m/s	0.4	0.0	0.4	0.1
max	m/s	3.2	-0.7	4.2	-3.5
p_{95}	m/s	0.6	-0.1	0.6	0.2
p_{99}	m/s	0.8	-0.4	0.8	-0.3
RL_{10}	m/s	3.1	-2.3	4.6	-4.3
RL_{50}	m/s	5.8	-4.4	8.3	-7.8
f_{20}	days	13.3	-10.2	16.1	-13.5
f_{25}	days	1.5	-0.9	1.8	-1.4

Table 5.1: *Performance statistics of modelled vs. observed summer (May to September) gusts. The observed data come from 22 inland observation stations in the Netherlands (see Figure 3.2). The model data were extracted at the nearest grid points. Negative MBE values indicate a lower model magnitude compared to observations.*

Earth data, which is further discussed in section 6.1, and already indicates a potential dependency of maximum summer gusts on temperature.

In the RACMO-hist run mean gusts are overestimated, whereas the maximum gusts are underestimated at 19 out of 22 stations (average MBE of -1.6 m/s), see Appendix A and Table 5.2. Possibly, due to the coarser resolution, RACMO maxima are smoothed over a larger region, which could explain both the low maximum values and the high mean gust speeds.

For all models' gust maxima, the RMSE is significantly worse than the MBEs. This can be explained by the low frequency and local nature of convective extremes as discussed further in section 5.1.2. At a particular station an extreme event can be observed but not modelled, and vice versa. The missing of an event in the model results in a high negative error at one station, whereas a missed observation at another location a high positive error. These would add up to a high average RMSE, but in the sign-weighted MBE they cancel out. Note that using a fuzzy verification method as described in section 4.2 could help reduce the RMSE, however, the MBE will likely not change as the statistic inherently describes the presence of a bias in the model.

The discrepancy of all models is especially large for RL_{50}, with a MBE of -4.4, -7.8 (Table 5.1) and -3.7 (Table 5.2) m/s for HClim-ERA, HClim-hist and RACMO-hist, respectively. Note that every model shows an underestimation of this statistic. The large magnitude of the metric especially for HClim-hist can be explained by the combined effect of underestimation of gust maxima and frequency, and their projection into the future. For RACMO the performance is better, likely attributable to a lower frequency bias. The underestimation of frequency is discussed separately in section 5.1.2.

5.1.2 Modelled frequency of extreme gust events

The number of summer days with gust speeds above 20 m/s is severely underestimated by HClim, with a MBE of -10.2 and -13.5 days for HClim-ERA and HClim-hist, respectively. These error statistics are better for the number of days above 25 m/s (f_{25}), though this is more a result of the limitations of these metrics: there are simply less events of this magnitude, as shown in Table 5.3.

		HClim-ERA		HClim-hist		RACMO-hist	
		RMSE	*MBE*	*RMSE*	*MBE*	*RMSE*	*MBE*
mean	m/s	0.5	-0.2	0.4	-0.1	0.9	0.8
max	m/s	3.2	-0.7	4.2	-3.5	3.0	-1.6
p_{95}	m/s	0.9	-0.6	0.8	-0.5	1.0	0.6
p_{99}	m/s	1.4	-0.9	1.7	-1.4	1.0	0.1
RL_{10}	m/s	1.8	-0.5	3.2	-2.9	2.1	-1.4
RL_{50}	m/s	4.2	-0.8	6.3	-5.4	5.2	-3.7
f_{20}	days	13.3	-10.2	16.1	-13.5	9.4	-4.6
f_{25}	days	1.5	-0.9	1.8	-1.4	1.6	-1.2

Table 5.2: *Similar to table 5.1, but this time for daily maxima values for a fair comparison between the 3-hourly output of RACMO to the 1-hourly HClim and observational data.*
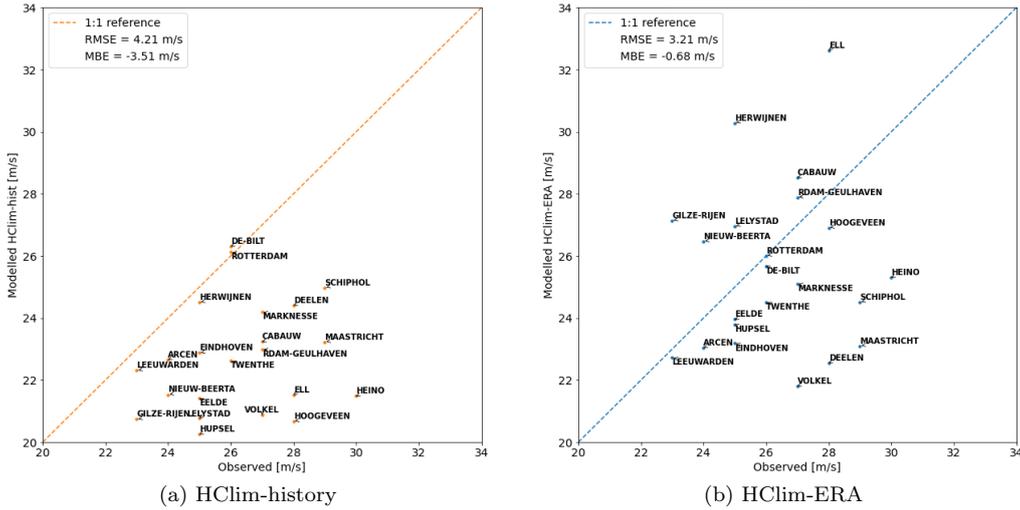

(a) HClim-history

(b) HClim-ERA

Figure 5.1: *Maximum of all summer (May to September) gust values of (a) HClim-history (1996-2005) and (b) HClim-ERA (2000-2009) versus observations (2000-2009) at 22 KNMI station locations (see Figure 3.2).*

The frequency of days with speeds above 20 m/s averaged over all station locations is 7.6 and 4.3 for HClim-ERA and HClim-hist, respectively, compared to 17.6 for observations. Above 25 m/s there are only 1.5 events on average observed per station, and 0.7 and 0.1 modelled for HClim-ERA and HClim-hist, respectively. Note that these numbers show that for HClim-ERA around 56% of the events above 20 m/s are missed, versus around 75% for HClim-hist. Interestingly, for RACMO the f_{20} compares much better to observations than HClim, with an average of 14.6 days compared to 17.6 days observed, corresponding to only 17% missed. See Figure 5.2 for a station wise comparison

for f_{20} in HClim-hist and RACMO-hist. A similar figure for HClim-ERA can be found in Appendix A.

		HClim-ERA	HClim-hist	RACMO-hist	Observations
days ≥ 20	m/s	7.6	4.3	14.6	17.6
days ≥ 25	m/s	0.7	0.1	0.4	1.5

Table 5.3: *Total number of summer days with gust speeds ≥ 20 m/s and ≥ 25 m/s in 10 years, averaged over the 22 locations (see Figure 3.2). Note that the total number of days in both model and observation data sets is 1530 (5 months, on average 30.6 days in these summer months, 10 years).*

A similar frequency bias was reported by Prein et al. (2017) and Liu et al. (2006) who studied MCSs using a CP-RCM, at a horizontal resolution of 4 km, in the United States. Even though the simulations were able to capture the key features of the MCSs, such as size, precipitation rates, propagation speed and lifetime accurately, their frequency was significantly underestimated at some locations. Prein et al. (2017) found that in areas with strong land-atmosphere coupling, in particular the Great Plains in the US, the MCS frequency was mainly underestimated in weak synoptic-scale forced conditions. Another explanation can be that the events missed are of small scale motion. Note that the studies of Prein et al. (2017) and Liu et al. (2006) investigated MCSs, which consist of a complex of organized thunderstorms. The resolution of CP-RCMs is however still too coarse to explicitly resolve smaller scale isolated thunderstorms, and these could be missed. The works of Tijm (2018) and Veen (2019) also reported an underestimation in the number of shallow showers in Harmonie. A more detailed discussion on the frequency bias can be found in section 6.2.

In RACMO, the number of days above 20 m/s compares much better to observations than HClim, with on average 83% of the events represented. Above 25 m/s the performance is equally bad, and above 31 m/s no events are recorded (see Figure 5.6 in section 5.1.4 below). Possibly, this can again be explained by the coarser resolution of the model: the peak gusts are smoothed over the grid cell resulting in a larger area of increased gust speeds, instead of finding more local maxima like with HClim. In addition, as mentioned in section 2.4.2, RACMO uses an extra term in the gust parameterization scheme when deep convection is identified by the model, which might outperform the higher resolution model HClim when gusts are not extreme (≥ 25 m/s) but still strong (20-25 m/s). The low frequency of extreme convective gusts with on average less than 1.5 events per location in 10 years poses a significant challenge for this study, and motivates the decision to aggregate data over larger regions.

5.1.3 Historical case study

This section analyses a historical case study to assess the ability of HClim to represent convective storms. For this analysis the maximum value of all used observation data is taken. The maximum gust summer value of all 22 observation stations between 2000-2009 is 30 m/s at Heino on June 8th 2003 at 12:00. The synoptic map of this date (Figure 5.3) shows a large high pressure system in eastern Europe and a low pressure system across the Atlantic. Warm air coming from the southwest was transported to northern Europe. This warmer air collided around noon with a cold front that reached the Netherlands. At Heino, the day commenced with little wind and after which it picked up around noon. At multiple locations in the Netherlands, the day was paired with severe thunder with locally more than 100 strikes per minute (KNMI, 2003). An animation of radar images as well
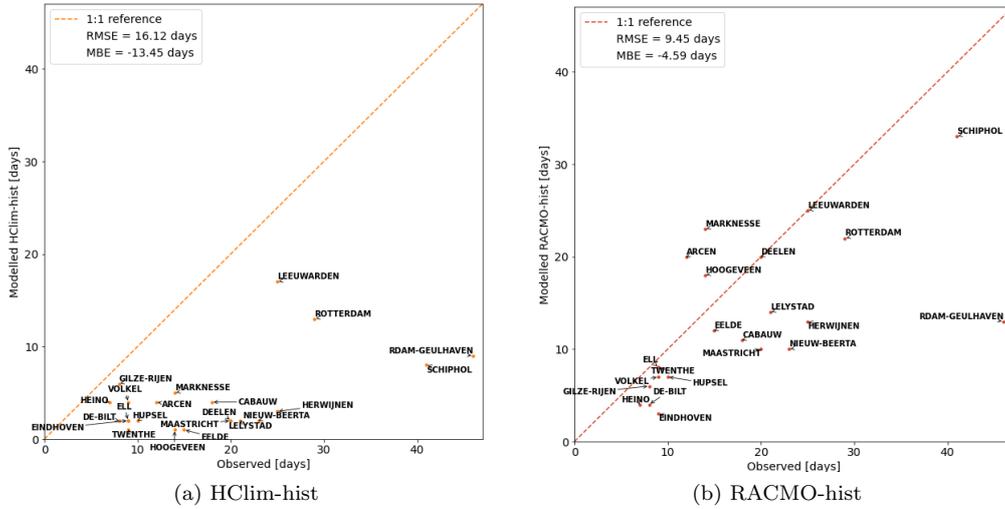
Figure 5.2: *Total number of summer (May to September, all model years) days with summer gusts above 20 m/s of (a) HClim-history (1996-2005) and (b) RACMO-history (1996-2005) versus observations (2000-2009) at 22 KNMI station locations (see Figure 3.2).*

as data from the KNMI lightning detection system of this date can be found in Appendix B. The historical data indicate that the observed extreme weather was paired with a mesoscale convective system consisting of multiple convective cells organized in a squall line.

The time series of this event is shown in Figure 5.4. At Heino, HClim-ERA misses the gust peak completely with no speeds above 11 m/s. The location at which the maximum occurred in the model is eastwards of Heino, and the time series as well as the location are shown in Figures 5.4 and 5.5, respectively. These figures show that even though the event is missed in the model at Heino, the model still resolves the storm but at a different location. This case study confirms the idea discussed in section 5.1.1 on where the high RMSEs for gust maxima originates. Extreme events are rare, especially when looking at point observations. At times, gust peaks are missed in observations and captured by the model, and vice versa. The local nature of summer events can explain the difference, and these results confirm the findings of Ebert (2008). Using a spatial and/or temporal window to include data surrounding the event relaxes the conditions for exact matches between forecasted and observed storms in time, intensity and space. In future studies assessing the performance of Harmonie Climate for extreme events it is important to bear this in mind. In section 5.1.4 data over a spatial box surrounding the Netherlands is aggregated.

This historical example indicates that HClim is able to capture complex convective storms organized as squall lines and confirms previous studies mentioning that CP-RCMs are able to accurately represent larger scale convective systems (Kendon et al., 2017). The accuracy of the extreme gust speeds modelled by HClim is more challenging to verify. The maximum observed summer gust speed at inland stations in the Netherlands between 2000-2009 is 30 m/s and does not come near the maximum HClim-ERA modelled speed of 45 m/s over all inland grid points of the box around the Netherlands (at 6.7°E longitude and 51.6°N latitude, on June 3rd 2005, nearest station Arcen). Possible explanations are that the high gusts in the model are too extreme, or that the most extreme events are missed by the stations.
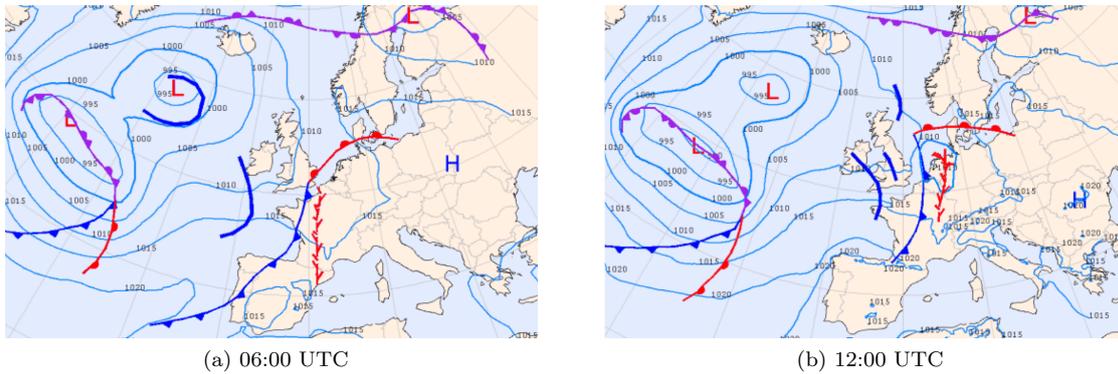
(a) 06:00 UTC   (b) 12:00 UTC

Figure 5.3: *Synoptic maps of Europe on June 8th 2003 by KNMI at 06:00 (left) and 12:00 UTC (right).*

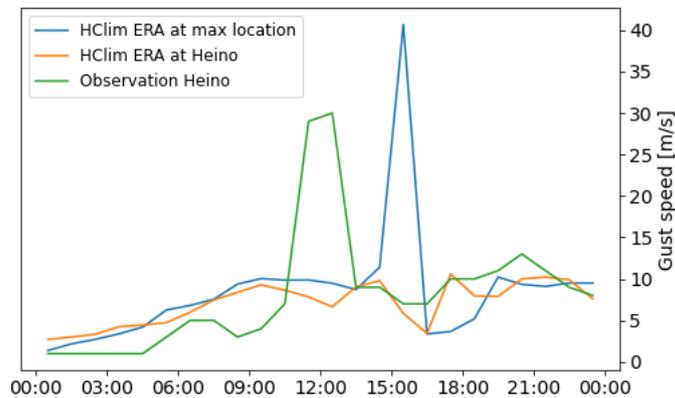**Maximum observed summer event on 2003-6-8: gust time series**

Figure 5.4: *The maximum inland summer gust observed between 2000-2009 was at Heino on June 8th 2003 at 12:00, with a speed of 30 m/s, as depicted with the green line. The HClim-ERA results extracted at Heino for the same day are shown with the orange line. The blue line indicates the time series of HClim-ERA from the location where the gust was maximum in the model at that day*

To test these hypotheses, the maximum modelled gust speed only at the locations of the observation stations is reported. This speed is 33 m/s at Ell, and compares reasonably well with the observed maximum in the same time frame 30 m/s at Heino. The maximum observed summer gust between 1950-2020 at the inland stations was recorded at station Schiphol, with a speed of 36 m/s, on the June 7th 1997 at 14:00. This event was the result of a quickly nearing cold front from the west, causing a MCS with bow echo structures (KNMI, 1997). The storm was paired with severe gusts and a few tornadoes, and resulted in large infrastructural damage and multiple casualties. Still, the maximum observed summer gust between 1950-2020 is 9 m/s lower than the modelled 45 m/s between 2000-2009. To study the ability of HClim to resolve extreme gusts in more detail, data of higher spatial density is required. Rawinsonde data could provide an interesting alternative to study thunderstorms individually (for example, Haklander and Van Delden, 2003).
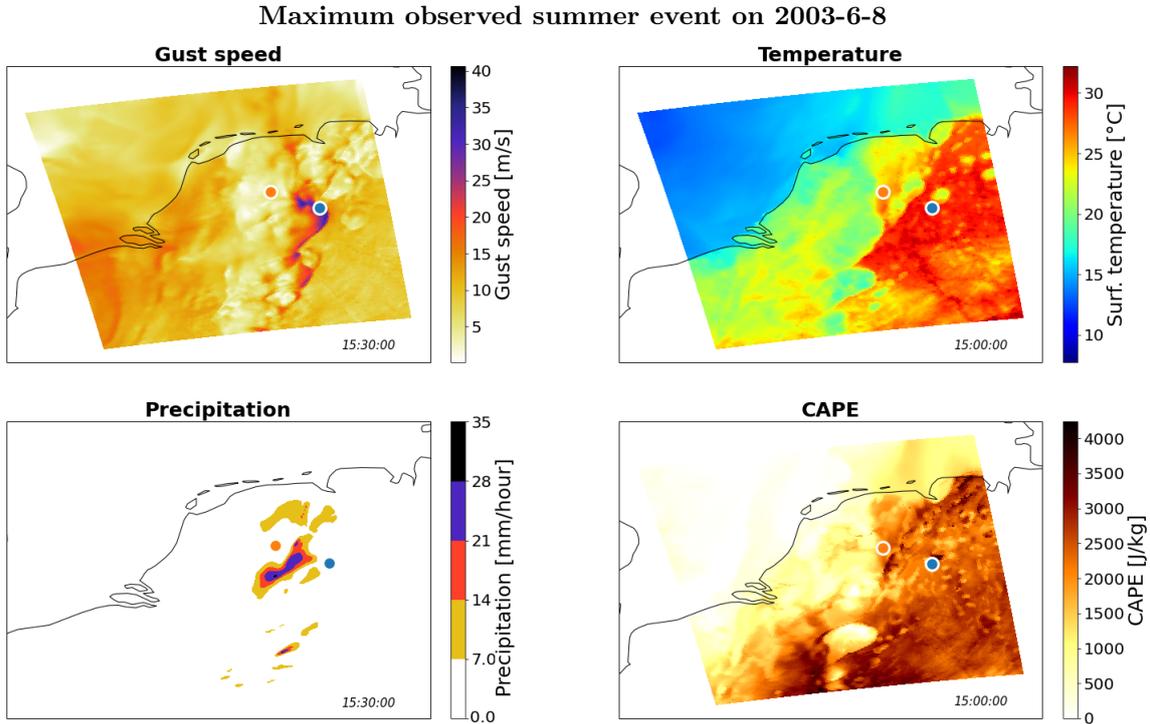
Maximum observed summer event on 2003-6-8

Gust speed

Temperature

Precipitation

CAPE

Figure 5.5: *The maximum inland summer gust of* 30 *m/s observed between 2000-2009 was at Heino on June* 8th *2003 visualised in HClim-ERA. The location of Heino is indicated with the orange dot, and the location of the maximum gust on that day in the model (at 15:30) is shown with the blue dot.*

5.1.4 Extreme events and model resolution

The number of extreme events happening in a larger region and not just in single grid points is further explored in the boxplot of Figure 5.6. For this figure, the maximum daily value for 10 years of summer data for points in the box around the Netherlands at least 25 km away from the coast is used. Note that the median, and 25th and 75th percentiles are roughly the same for the HClim runs, with slightly lower RACMO values. Note that this might seem like a contradiction with the results found in section 5.1 where RACMO showed a positive MBE for the p$_{95}$ and mean statistics when compared to observations, and the HClim runs a negative MBE.

One should keep in mind however while this analysis regards the entire non-coastal Netherlands, that analysis was based on 22 grid points. The main difference is the magnitude of the outliers. In all HClim runs, the magnitude of the highest outlier surpasses the magnitude of the highest outlier of the RACMO runs by at least 8 m/s. None of the RACMO values pass 31 m/s, whereas the HClim runs all have 10 days or more above this value. The variation amongst the HClim runs becomes visible when zooming into the top outliers, and the differences between these runs are further explored in the next sections.

The dissimilarity between runs forced with various GCMs is discussed in many studies using an ensemble of GCMs. For example, Rädler et al. (2019) found that the RACMO-EC-Earth RCM was on the low end of climate change impacts by the end of the century relative to other models. This

stresses the strong disadvantages of relying on the prediction of a single model. A large issue is computational expense when performing model runs at convection permitting scales. However, as indicated before, hydrostatic RCMs do not seem capable of capturing convective extremes. Therefore, the benefits of using a single CP-RCM for such studies possibly outweigh the usage of multiple conventional RCMs. To summarize, the statistics show an increase in extreme gust magnitude and frequency in a warming climate, but as using a single GCM comes with large uncertainty, the magnitude of these projections should be taken with precaution.
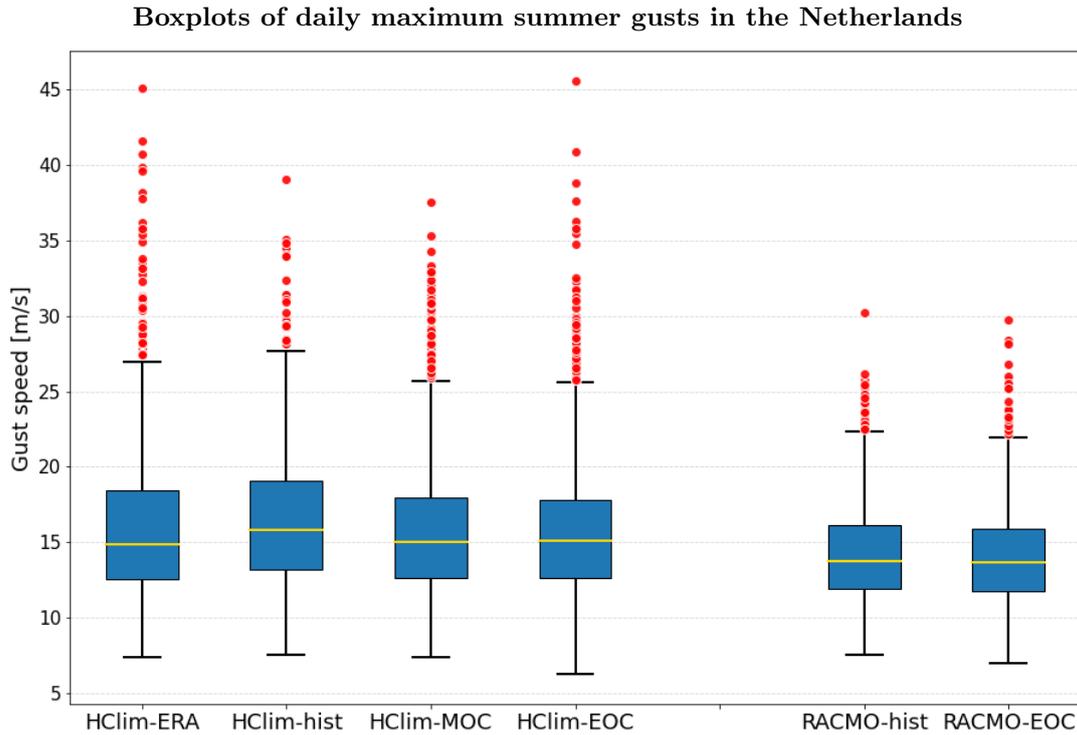
Boxplots of daily maximum summer gusts in the Netherlands

Figure 5.6: *Boxplots of the daily maximum gust speeds over the Netherlands over land (≥ 25 km away from the coast) in the 10 years of summer months in each model. The yellow line represents the median value. The bottom and top of the blue box the 25th and 75th percentiles, respectively. The upper tail is the 75th percentile plus 1.5 times the difference between the median and 75th percentile. The lower tail is the 25th percentile minus 1.5 times the difference between the median and 25th percentile. Daily maxima beyond the whiskers are considered outliers and are plotted as red dots.*

5.2   Future runs analysis: climatology

This section aims to address to what extent convective gusts will change in a future warmer climate through an extended climatological analysis (research question C1). The boxplots of Figure 5.6 already give a good indication for changes in the future by studying the differences between the HClim runs. The HClim-ERA and HClim-EOC run both contain around 10 days with extremely high wind speeds above 40 m/s and up to 45 m/s, whereas HClim-hist and HClim-MOC only have two. The highest gust speed is found in the HClim-EOC run, with a speed of 46 m/s. There is

an increasing trend of summer days with gusts above 30 m/s when going from the HClim-hist to HClim-MOC to HClim-EOC run. This could indicate that extreme gusts will become more common in the Netherlands in a warmer climate, though the inherent low frequency of extreme events poses a challenge to distinguish natural variability from an actual trend. To extend the data set, the next sections not only look at gusts in the Netherlands but on the entire European continent. The statistics used are p_{95} and maxima, and days with gusts above 20 and 25 m/s, in Figure 5.7 and 5.8, respectively. Note that in these figures the contours are closed at the top. For example, the filled region between 0 and 1 means $0 < x \leq 1$, and the leftward pointing arrow of the color bars hence indicates $x \leq 0$.

5.2.1 Summer gust 95th percentile and maximum value

Figure 5.7a shows the p_{95} value of the daily maxima of gust in summer months over Europe for the RACMO and HClim history runs and changes between history and end of century runs. The figure confirms that wind climatology strongly depends on the geography and terrain characteristics of a region (for example, Jiménez and Dudhia, 2012). The history runs have comparable p_{95} values for inland Europe and at sea. Locally, the differences between the models are remarkable. The HClim run shows significantly higher p_{95} values at the Mistral-reigned Mediterranean near southeast France. Here, p_{95} are up by 10 m/s compared to other regions in the Mediterranean. In RACMO, this local increase is hardly visible. Similarly, HClim shows significantly higher p_{95} in the high Pyrenees and Alps, with locally values higher than 25 m/s compared to values below 18 m/s for inland Europe with little orography. In RACMO, the increased values in the mountainous areas are not represented. Compared to the history run few changes are visible in the RCP8.5 end of century runs. For both models, in most of inland Europe the difference is between -1 and 1 m/s. Especially in the HClim run only few small regions, in the high Alps, show an increase of more than 3 m/s.

In Figure 5.7b the maximum value of every grid cell in ten years of summer data is shown. Note that one event can occur multiple times in one figure as it moves spatially over the domain. In the history runs the maximum wind speeds for inland central Europe range between 19 and 30 m/s. The spatial variations in inland Europe of the maximum value regardless of orography contrast with the mostly uniform p_{95} field. The HClim history runs shows a few small points with speeds up to 41 m/s, and in mountainous regions the maximum summer gust exceeds 45 m/s. In the historical RACMO run these orographic and local inland maxima are not resolved: in terrestrial Europe wind speeds do not pass 30 m/s, with few exceptions up to 38 m/s in the Alps and Pyrenees.

Interesting differences are visible between the HClim-Hist and HClim-EOC runs in central inland Europe particularly. Over almost the entire mainland terrestrial Europe the maximum wind speed increases. Locally, especially in Germany, the increase is beyond 20 m/s. These local clusters are connected to independent local storms of a few kilometers in size with extreme wind speeds (up to 47 m/s). Besides becoming more widespread, the clusters additionally seem to become larger. Note that the change in eastern Netherlands, eastern France and Germany is especially large. In RACMO, the change in maximum wind speed generally stays between -5 and 5 m/s, with one exception in the western Alps, where the maximum gust is increased with 15 m/s. At sea, RACMO and HClim show similar patterns: the wind maximum speed decreases slightly (up to 10 m/s), except for the southern North Sea, where gust speeds are increased up to 10 m/s.

Thus, the difference between using CP and hydrostatic dynamics is especially evident in complex terrain, such as the central Alps, Pyrenees and Mistral region of southeast France. This study focused mainly on the Netherlands where little topographical variation exists. The benefits of using a high resolution CP-RCM might be even higher in regions of higher complexity (for example,

Vanden Broucke et al., 2019). In future studies, these areas should be addressed separately and with observed data included.

### 5.2.2 Projections in frequency of summer days with strong gusts

Figures 5.8a and 5.8b indicate how common high gust events are by showing the amount of summer days with gusts above 20 (f_{20}) and 25 m/s (f_{25}), respectively, in the 10 years of model data. The spatial patterns, especially for f_{20}, resemble those of the p_{95} value as seen in Figure 5.7a. Both history runs show that most of terrestrial Europe has between 1 and 50 summer days with gusts above 20 m/s, and the HClim run shows increases for mountainous and the Mediterranean Mistral regions of between 100 and 1000 days.

The HClim runs show an increase of the f_{20} going from the history to end of century run in mainland terrestrial Europe of between 2 and 10 days. Both models indicate an especially strong increase above Denmark in the RCP8.5 scenario. In contrast, at the North Sea, eastern Atlantic and Mediterranean the f_{20} decreases with 2 to 20 days. Also above western France and southern UK the number of stormy days decreases.

The above 25 m/s field in Figure 5.8b is less uniform. Most of inland non-mountainous Europe is characterized by 1-2 and maximum 5 events that follow a similar spatial pattern as the maximum values of Figure 5.7b. For all model runs the marine regions mimic the p_{95} pattern better, where the Mistral winds and areas with high topographic complexity are better captured by the HClim runs. These figures confirm once more how scarce extreme events are for a single grid point. This brings along challenges to distinguish the natural variability from observed trends, as further discussed in section 6.2.
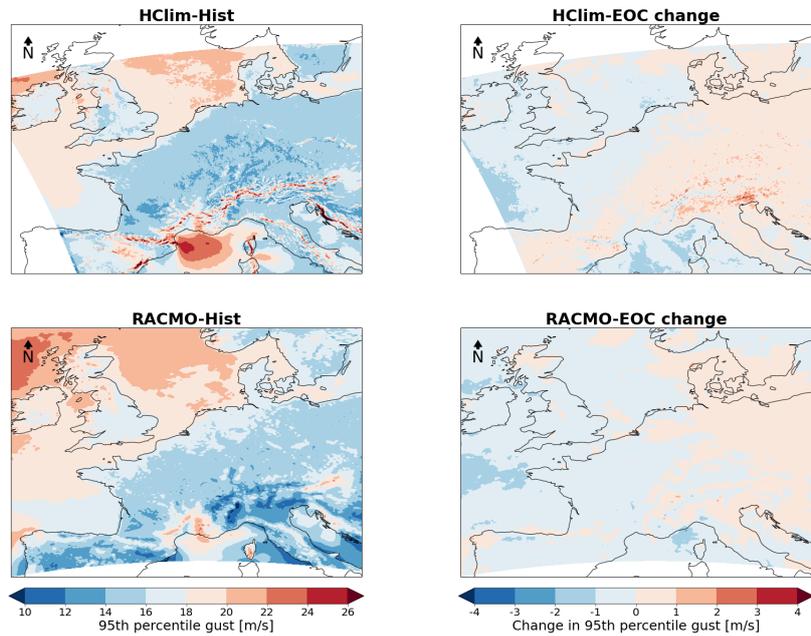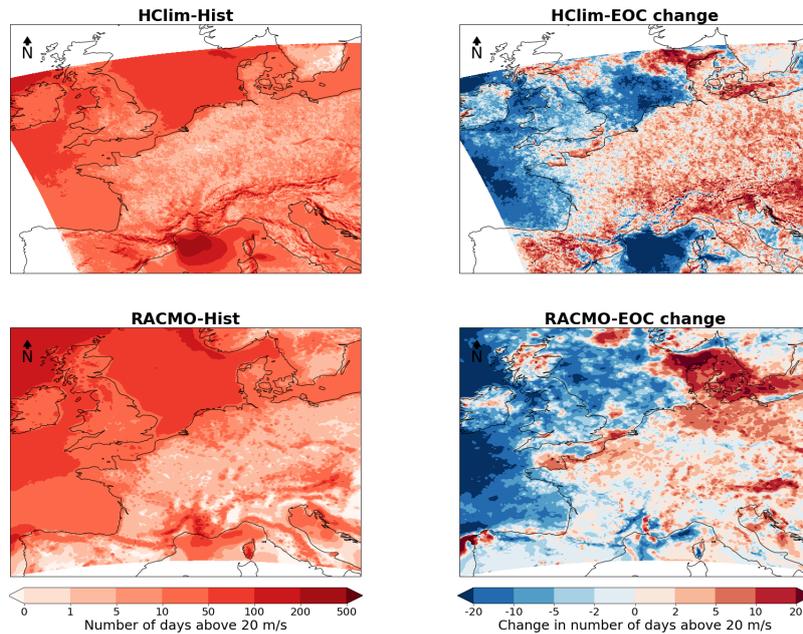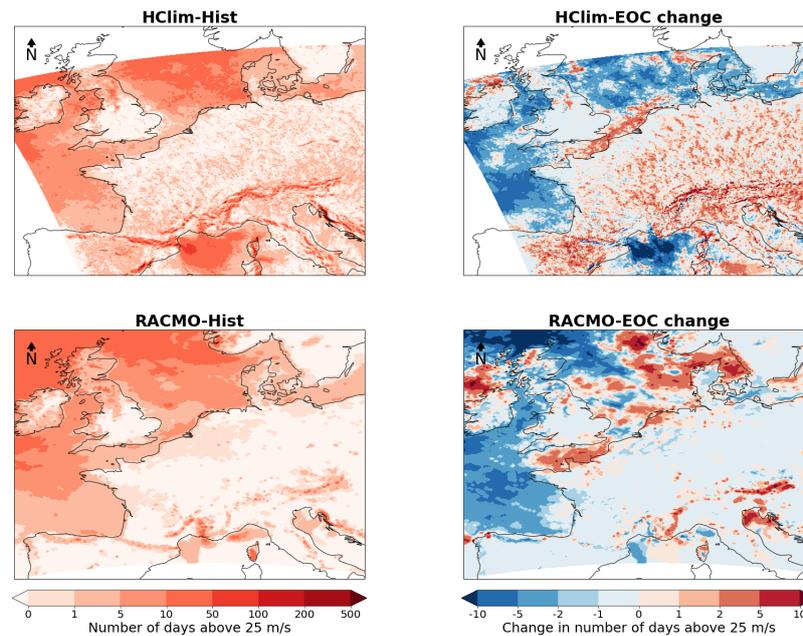
(a) 95th percentile summer gust
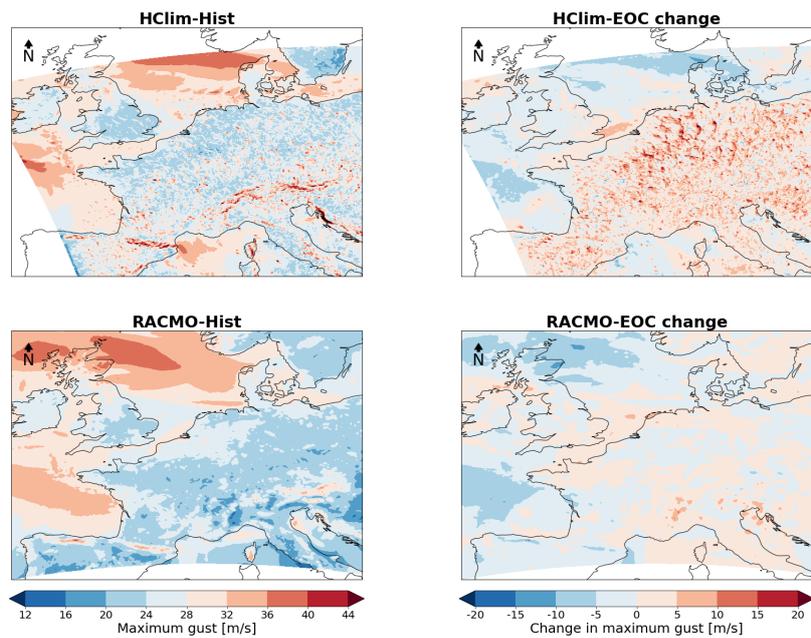
(b) Maximum summer gust

Figure 5.7: *Summer gust (a) 95th percentile of daily maxima and (b) all time maxima in the 10 years of model data in the RACMO and HClim history runs (1996-2005, left two figures) and change compared to the history runs in the RCP8.5 scenario (2090-2099, right figures): EOC minus history.*

(a) Days with gusts $\geq$ 20 m/s

(b) Days with gusts $\geq$ 25 m/s

Figure 5.8: *Number of summer days with gusts (a) $\geq$ 20 m/s and (b) $\geq$ 25 m/s in the 10 years of model data for the RACMO and HClim history runs (1996-2005, left figures) and change compared to the history runs in the RCP8.5 scenario (2090-2099, right figures): EOC minus history.*

5.3 Future runs analysis: case studies

In this section the fate of convective gusts in a future warmer climate is addressed from a more dynamical perspective by looking at case studies (research question C2). For this analysis, ten extreme convective gust cases are selected for the HClim-hist, HClim-EOC and RACMO-EOC run as described in section 4.3. For comprehensiveness, this analysis is focused on the Netherlands. Of the selected cases, three are discussed in more detail in the next sections. Two of these are maximum events in the HClim-EOC run and one in the RACMO-EOC run. Note that the selected cases in fact correspond to the gust values of the red dots of the boxplots of Figure 5.6. Animations including 7 (RACMO) to 9 (HClim) atmospheric variables of all thirty events can be found on an external drive, see Appendix B. In this section spatial plots in time are shown from the time when the gust in the events was maximum, as well as time series of all parameters over time at the location where the gust was maximum during the day. In addition, the environmental conditions of all case studies are analysed through boxplots.

5.3.1 HClim future case 1

The first selected event from HClim-EOC is takes place on the on the 29th of June 2097 and is shown in Figure 5.9a and the same date in RACMO in Figure 5.9b. The time series are shown for both models in Figure 5.10. In HClim the day is characterized by very warm surface temperatures, already starting at $28°C$ in the south of Netherlands at midnight, increasing up to $35°C$ by 8:00 and reaching its maximum around 13:00 when most of the country experiences temperatures between $42°C$ and $45°C$. This is higher than any temperature experienced so far, with a current Dutch record of $40.7°C$ (KNMI, 2020). The high temperatures are contrasted with dewpoints of below $10.0°C$, indicating a low relatively humidity ($< 15\%$).

By 14:30 a small amount of precipitation of maximum 7 mm/hour occurs in local clusters, which develop into larger showers of maximum 15 mm/hour, until 17:30 they disappear from the domain. At the location where the gust was maximum, the precipitation did not exceed 1.0 mm/hour. Note that the intensities can be higher locally and at a certain time as the variable indicates the total precipitation that fell over the hour; the amount might have fallen within a few minutes. The development of the showers happens simultaneously in location and time with the growth of several cells with decreased temperatures. At 15:00, some of these cells have a temperature drop of $20°C$ compared to their surroundings and previous time steps. Simultaneously, at the location of the convective cells the dew point temperatures increase to similar magnitudes, indicating saturated air.

The shape of the cold pools are mimicked by the vertical wind at 925 hPa. The vertical wind hints that the cold air is coming from higher levels, as the center of the pools indicate down going flow whereas the rims show upward velocities. This exchange of air is also indicated by the close-to-zero wind shear values at the location of these cells, whereas the shear is high (up to 40 m/s) in other regions. The positions of the maximum wind and gust fronts coincide with the rims of the cold pools. The time series of Figure 5.10 show how closely the wind speed and gust speed are related, where it seems that the gust speed is simply the wind speed and an added term, despite the latter being the maximum value over the hour and the former an instant value.

The CAPE increases in the morning and reaches a maximum for most areas in the Netherlands around 2500 J/kg, and locally up to 6000 J/kg at the IJsselmeer. The CAPE drops for most of the country after the storm passage to values below 700 J/kg. The cell-structured footprint with multiple convective updrafts and downdrafts of this event mimics the theory of the multicell storms as discussed in section 2.1.3. This fits with the observation that the gust fronts are caused by the result of the interaction of the cold pool boundary and the environmentally unstable air. As expected

43

from theory (Lin, 2007 and Markowski and Richardson, 2011), the cell structures are moving towards the downwind side of shear.

Noticeably, many of the ten EOC events are paired with high temperatures, strong shear and high convective instability, and makes the event on 29th of June 2097 a good example for the end of century run. The storm is triggered by a convergence line with wind and cooler air from the west side, with gust bow echos forming the front of the convective front. Assuming an air temperature drop of 9.8°C per 1000 m altitude, and for the dew point 1.8°C, the low dew point temperatures (≤ 8°C) in combination with high air temperatures (≥ 42°C), would locally indicate a convective cloud base of 4.2 km. The associated latent cooling would easily allow for downbursts and extreme gusts speeds. Such extremes are not observed in the current climate in the Netherlands (Haklander, 2020).

The development of temperature and pressure for this day are somewhat resembled by RACMO as visible in Figure 5.9b, 5.10 and the animations, though differences exist. The temperatures in RACMO are not as extreme as in HClim and do not exceed 40°C. The maximum gust speeds are only half of the maxima in HClim with a maximum in RACMO of 20 m/s for this day. The discrepancy in temperature can potentially be explained by the saving of variables at 3-hour intervals and simply missing the time when temperatures are highest. This however does not explain the difference between HClim and RACMO for gusts as the parameter is written away as the maximum of the passed three hours. RACMO also indicates relatively low dew point temperatures compared to air temperatures and minimum precipitation amounts. The cold pools or convective cell structures that are clearly visible in the temperature, gust, wind and pressure fields of the HClim run are absent in RACMO. Figure 5.9b does show a large region with gust speeds between 17 and 22 m/s, much larger than the area in HClim with gust speeds of the same magnitude. This supports the idea that in RACMO gust maxima are spread out over a larger region in a smoothing effect. The more extreme gust speeds above 22 m/s are however completely missed by RACMO.

5.3.2   HClim future case 2

The maximum event in HClim-EOC on the 24th of July 2091 (see Figure 5.11) has some characteristics that resemble the first case: temperatures are high throughout the day, reaching up to 40°C around noon, shear is strong (up to 30 m/s), CAPE values are high (≥ 1500 J/kg in most areas, reaching up to 6700 J/kg locally) and the wind is coming from the west. The dew point temperature shows a strong contrast with surface temperature: around 11-14°C just before the storm develops, when it quickly increases to between 19 and 22°C at the center of the cell. The warm temperature field is once again interrupted by a growing cold pool where precipitation falls with rates op to 25 mm/hour. Again, the gust, horizontal wind and vertical wind fields mimic the shape of the cold pool, that initially is one large cell and later accompanied with a smaller one.

The parameters on the same day in RACMO are shown in Figure 5.11b and time series in Figure 5.12. RACMO resembles the increase to temperatures of locally up to 40°C and subsequent drop well, as well as the pressure, CAPE and dew point temperature fields, though misses the high wind and gust speeds, as well as the local colder cells. Throughout the day the gust speeds of RACMO are higher at the location where gusts are maximum, except at the peak around 15:00. Similarly, the peak is missed in the mean wind speed time series. RACMO does show an area with increased gust speeds (13 - 22 m/s) and covers a larger area than the area with the same magnitude in HClim, even though in RACMO this area is located further to the southwest. Within the increased wind speed region, RACMO misses the extreme speeds exceeding ≥ 31 m/s.

Case study 1 on 2097-6-29
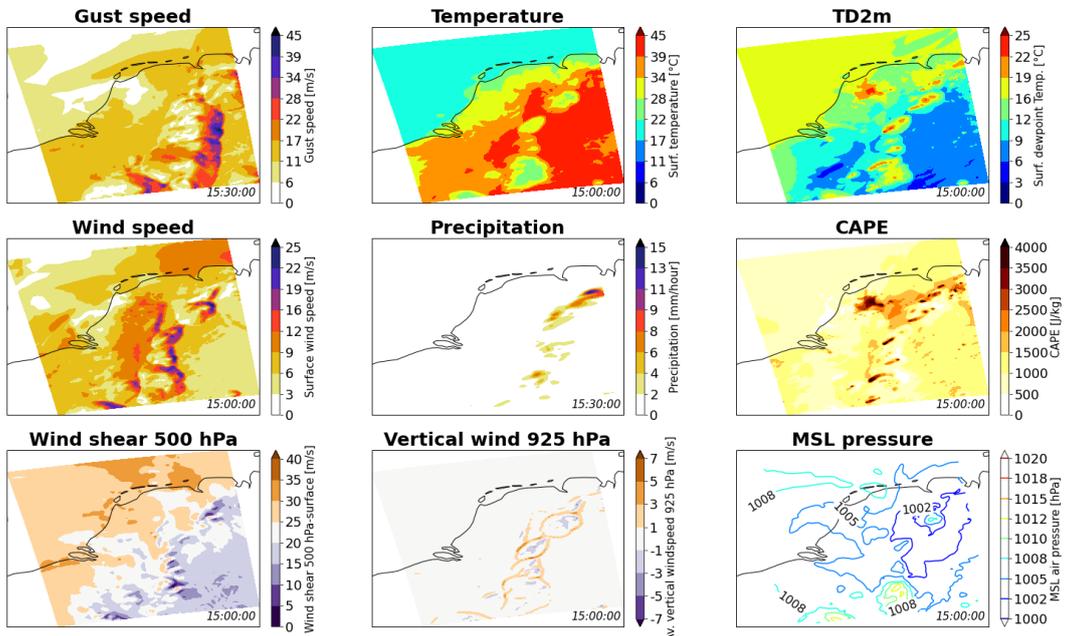
(a) HClim
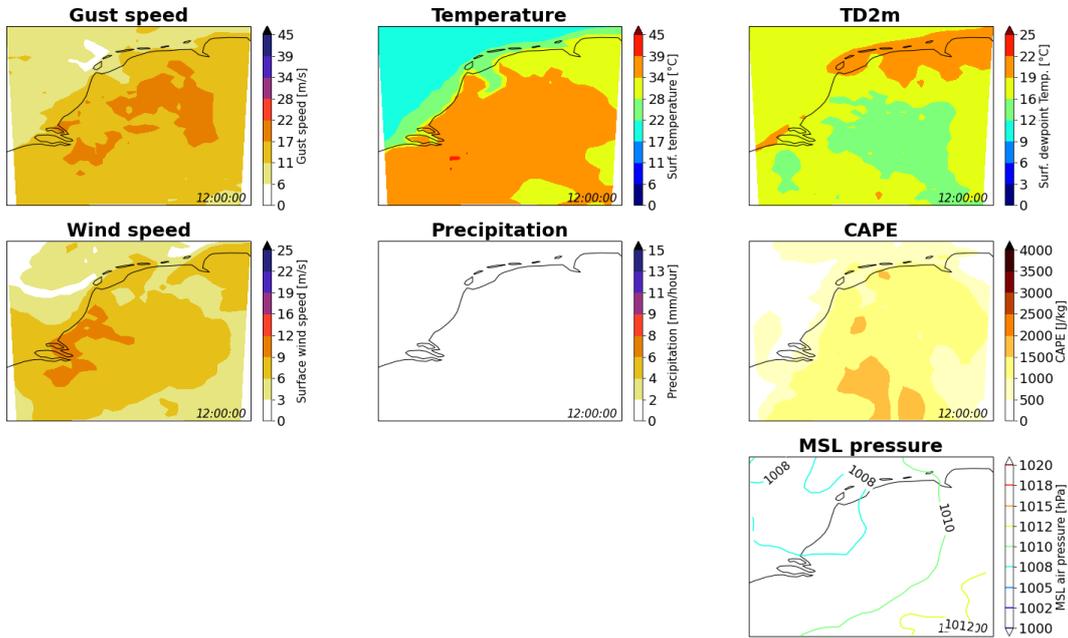
(b) RACMO

Figure 5.9: *Case study on the 29th of June 2097, one of the top 10 maximum convective events depicted in the HClim-EOC run in (a) HClim (b) RACMO.*
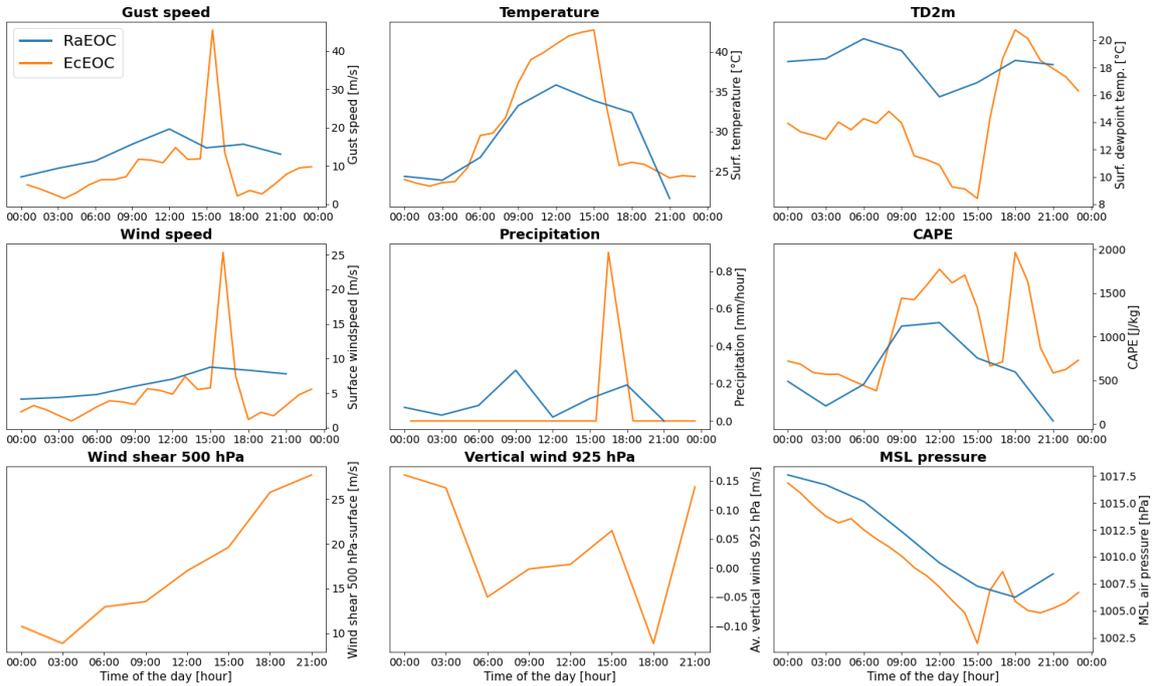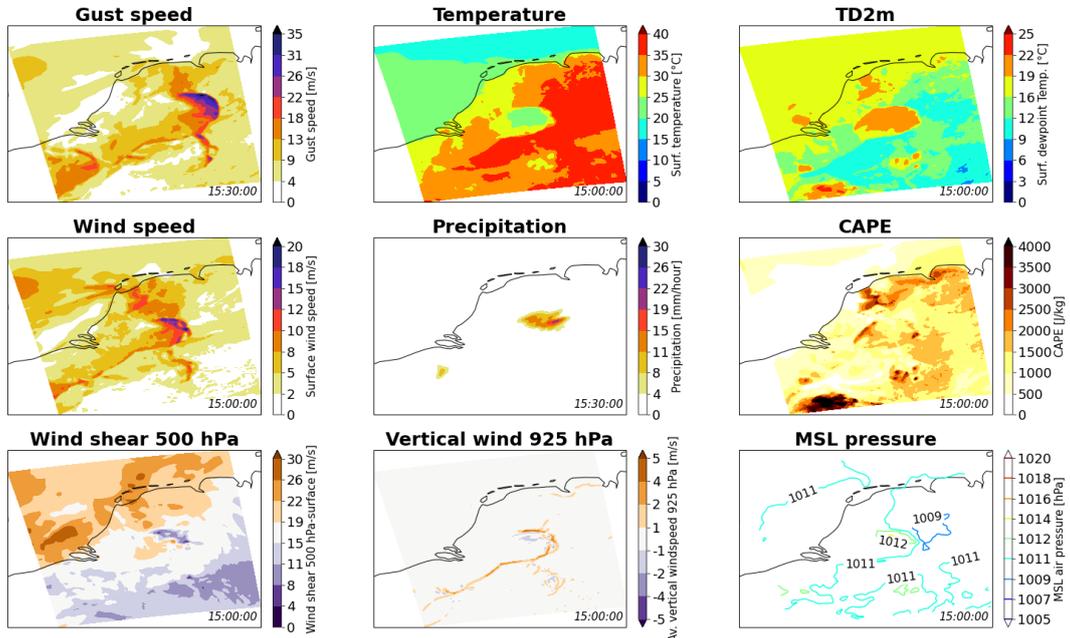
Figure 5.10: *Time series of variables of case study on the 29th of June 2097, one of the top ten maximum convective events in the HClim-EOC run. The location of the time series is stationary and taken at the point where the gust of the event was maximum during the entire event. For HClim-EOC this is at 7.6° E longitude and 51.2° N latitude, for RACMO-EOC 6.7° E longitude and 52.5° N latitude.*

### 5.3.3   General characteristics HClim's maximum events

In Appendix B animations of the 10 maximum events in and HClim-hist and HClim-EOC can be found. Figure 5.13 shows statistics of the environmental conditions of these events. From these resources interesting results will be shown. First, all twenty cases take place between May and September: 2 in May, 5 in June, 2 in July, 6 in August and 5 in September. This indicates that the choice of limiting the analysis for convective extremes to May to September is justified.

Second, all maximum HClim-EOC events take place on days with high surface temperatures. Seven out of ten case studies are paired with temperatures locally up to 40 and for two events even up to 45°C. The p_{95} temperatures of the entire day of all EOC events are above 25°C, with an average of 33°C. These numbers are significantly higher than the p_{95} temperature of an average day, at 22°C. For the HClim-hist case studies the temperatures are significantly lower: in only three events temperatures locally pass 30°C and in some events the p_{95} is lower than the p_{95} for an average day. The hotter three events are all in the top four in terms of gust speed. The higher temperatures possibly increase the instability of the atmosphere, and hence increase the potential for deep moist convection. Indeed, in all case studies, the p_{95} CAPE is much higher than on an average day. In the EOC case studies, some CAPE value are locally up to 8000 J/kg. The three historical cases with highest temperatures and gust speeds also relatively have the highest maximum CAPE.

Case study 2 on 2091-7-24

(a) HClim
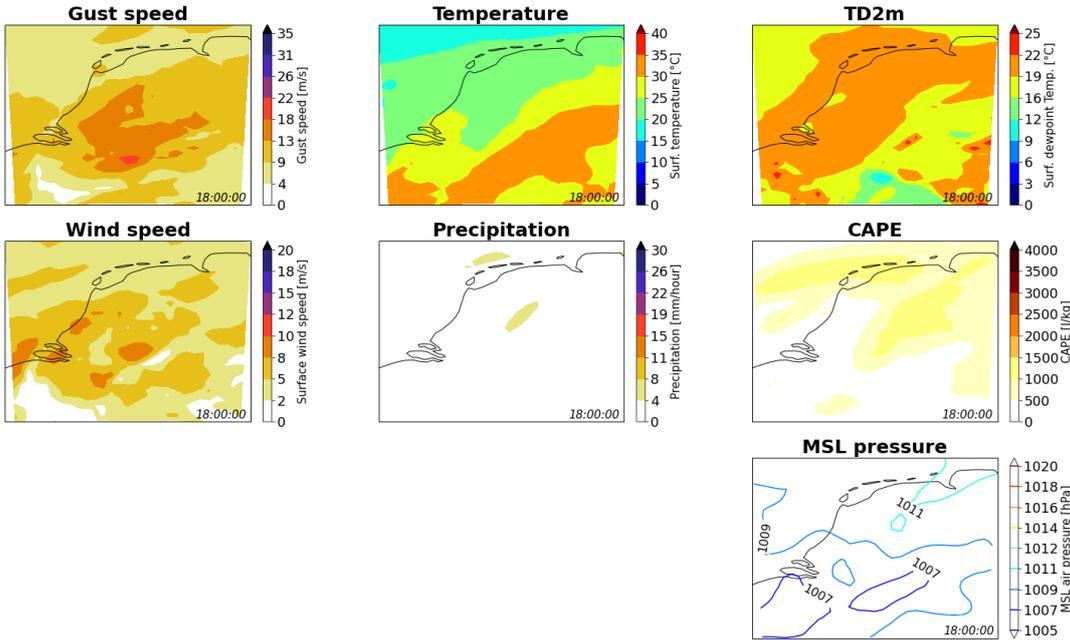
(b) RACMO

Figure 5.11: *Case study on the 24th of July 2091, one of the top 10 maximum convective events depicted in the HClim-EOC run in (a) HClim (b) RACMO.*
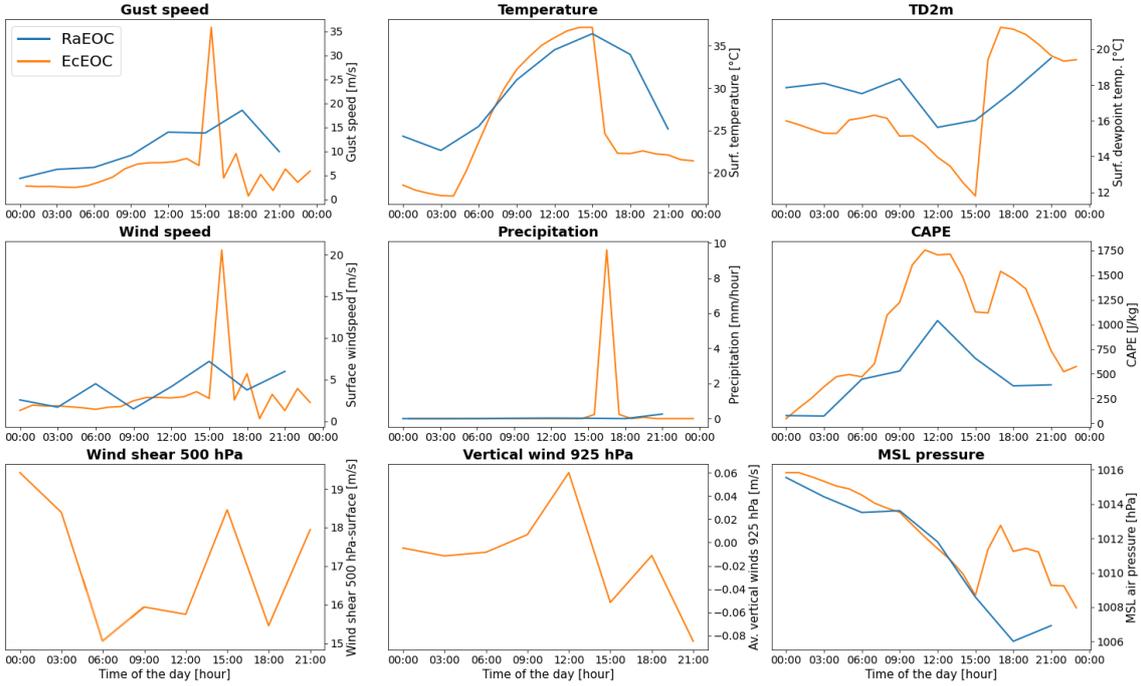
Figure 5.12: *Time series of variables of case study on the 24*th *of July 2091, one of the top ten maximum convective events in the HClim-EOC run. The location of the time series is stationary and taken at the point where the gust of the event was maximum during the entire event. For HClim-EOC this was at 7.1° E longitude and 52.5° N latitude, for RACMO-EOC 5.5° E longitude and 51.0° N latitude.*

Note that in the HClim-EOC run the maximum CAPE values are higher than the historical cases. The values for an average summer day, both in terms of maximum and p_{95}, do not differ much for an average day between the two runs. It could still be that there are more days with high CAPE values, or that CAPE is increased during some periods of the day, or that there are more days with high CAPE and increased shear. Note that these average values merely give an indication of a normal day. An extensive analysis of trends in the environmental parameters for extreme convective conditions is left out of this study, as the works of Rädler et al. (2019) and Púčik et al. (2017) have already extensively discussed potential changes of instability in Europe.

The spatial dew point temperature development varies amongst the cases. On some days, right before the gust front comes in, high surface temperatures are contrasted with low ($< 10°$C) dew point temperatures, at some locations and time steps the contrast is more than 30°C, allowing for strong evaporation rates. From the animations the source of moisture is not clear and could come from higher levels. At the moment the storm front passes, the surface temperatures at the location of the convective cells decrease simultaneously with an increase in the dew point temperatures, until they are around the same magnitude, indicating nearly or completely saturated air. The temporally low surface dew point temperatures of some cases are not reflected well in the higher p_{95} value of Figure 5.13, that is likely more influenced by higher dew point temperatures at other regions or

after the gust front passed. Note from Figure 5.13 that the dew point temperatures of the EOC run are higher compared to the historical ones. This could mean that more moisture is paired with the end of century events. Note that the p_{95} dew point temperature for an average day also increases towards the end of the century.

In most HClim events, the p_{95} shear can be classified as moderate to strong (see section 2.2.2). Around the gust fronts, in almost all EOC events, the shear is around 40 m/s with a median around 30 m/s, especially on the windward side of the convective cells, on the downwind side the values are usually lower (< 10 m/s). The time after the events can cause the lower p_{95} shear when taken over the entire day. There is one event in the EOC run (on the 24th of June 2097, see Appendix B) where shear values do not cross 15 m/s during the day, at all locations. The spatial characteristics as seen in the animation of that day do indicate a mesoscale convective system with multiple convective cells. Why the shear remains low in this case is not exactly clear. When looking both at the maximum and p_{95} shear the values of the historical cases are higher compared to the EOC cases. This can potentially be explained by increased stability and less shear required to initiate long lasting convective systems.

Note that the p_{95} of the surface wind field for the historical runs is higher compared to the EOC runs. In addition, the historical case studies are paired with lower mean sea level pressures compared to the EOC run. This indicates that the historical case studies can be more related to the synoptic situation with lower pressure systems and already strong mean wind. In the EOC run the gusts are more local, with sudden wind gust increases. This shows the importance of not only looking at the wind field but in addition at gust speeds. In all of these events, the wind is coming from west to southwest. With few exceptions the location of the maximum gust speeds is near the border with Germany.

Interestingly, not all extremes are paired with significant precipitation, indicating that the findings of more commonly studied projections in extreme precipitation cannot be applied directly to gusts. The maximum vertical wind speed remains below 6 m/s both upwards and downwards. This is significantly slower than the 40 m/s downdrafts recorded in tornadoes (Markowski and Richardson, 2011). Though, in the observed case, the downdrafts are over a region of a few hundred meters and not 2.5 km. The model resolution of 2.5 km is still too coarse to resolve tornado and waterspout events.

5.3.4   Short conclusion from HClim's maximum events

These results show that the convective storms found in the HClim runs resemble the theory described in Chapter 2. Namely, all case studies are paired with high CAPE values and almost all with strong shear. Besides, the animations of the cases, especially in the EOC run, resemble the shape of mesoscale convective systems and squall lines in particular. This supports the hypothesis that HClim is capable of capturing local extreme convective storms and their complex and multi and supercell structures.
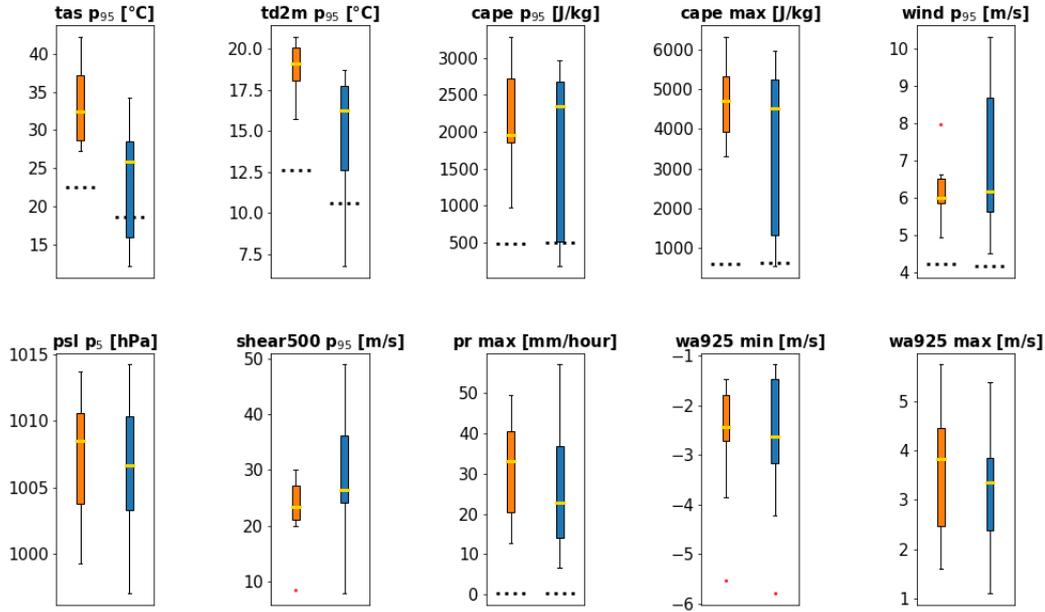
Figure 5.13: *Environmental conditions over land of 10 case studies in HClim-EOC (orange) and HClim-hist (blue) in the Netherlands. The dotted lines represent the value of the statistics for an average summer day in the Netherlands. Note that the data required to calculate the mean climatological statistic are not available for the the mean sea level pressure and vertical wind speed. The boxplots are computed in the same way as Figure 5.6.*

5.4 The RACMO case studies

5.4.1 RACMO future case

The spatial characteristics of the RACMO-EOC maximum event on August 31st 2099 are shown in Figure 5.14a in RACMO, and Figure 5.14b in HClim. The time series are shown in Figure 5.15, and animations of the environmental variables for this date can be found in Appendix B. An inspection of the time lapses of these events reveals that the storm is governed by a low pressure field moving across the north of the Netherlands. The wind speed direction is parallel with counterclockwise direction to the isobars, as expected from geostrophical principles. In both HClim and RACMO no clear development of cold pools is visible. In HClim and RACMO, at the location of the wind speed maximum the day starts with moderate surface temperatures of around 18°C and increase up to 30°C around noon. After the storm passed, the temperatures drop to around 20°C. The dew point temperature and CAPE values follow a similar pattern, with increases till noon and decreasing values towards the end of the day, from 12 to 16 to 10°C for dew point and from 0 to 1000 to 100 J/kg for CAPE. The pressure follows the opposite trend starting at 1007 hPa at the beginning of the night, to a minimum of 1000 hPa and later increasing to 1005 hPa. Very little precipitation (≤ 1 mm/hour) is modelled. The gusts in HClim go up to 30 m/s around 14:00, proceeded and followed by little wind, $<$ 10 m/s. In the RACMO run the day starts and ends quiet too, except for the values at 9 am, 12 pm and 3 pm when gust speed pass 15 m/s though never go beyond 20 m/s.

Case study 3 on 2099-8-31
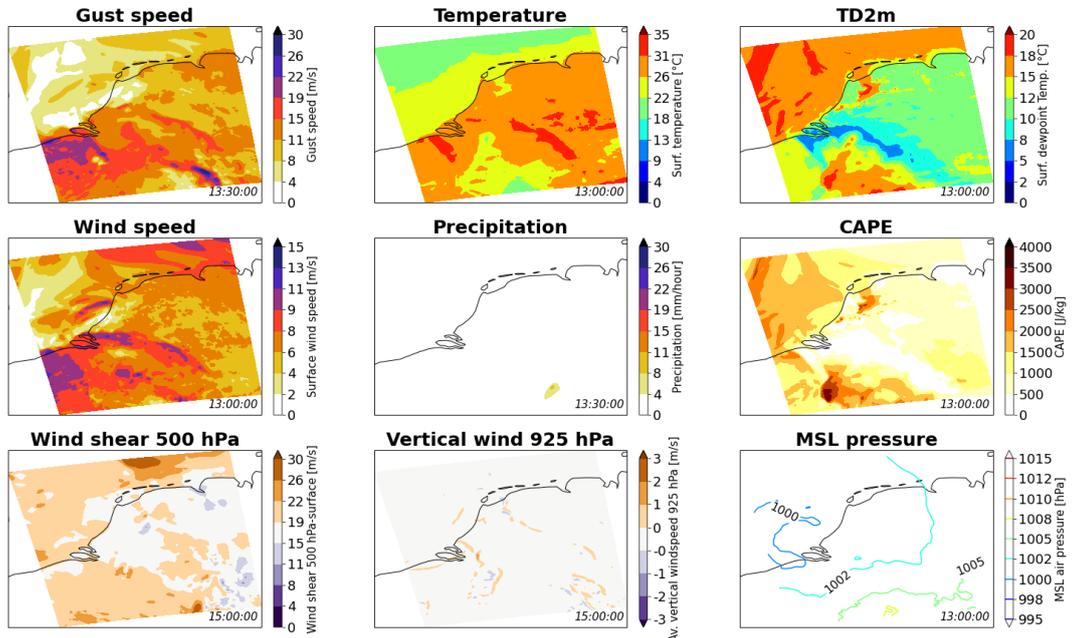
(a) HClim
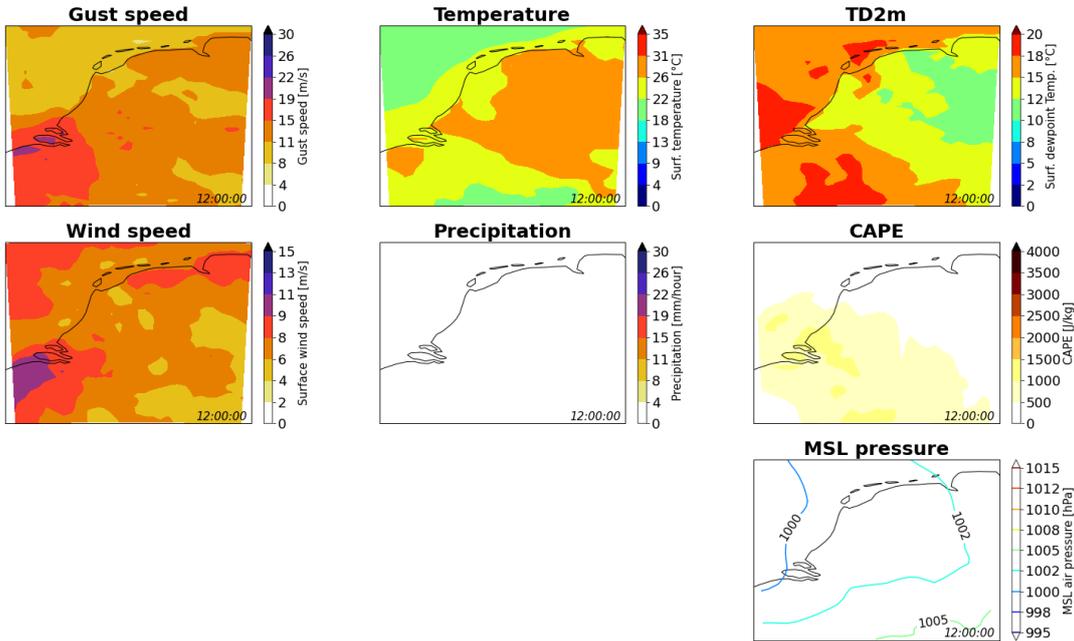
(b) RACMO

Figure 5.14: *Case study on the 31st of August 2099, one of the top 10 maximum convective events in the RACMO-EOC run depicted in (a) HClim (b) RACMO.*
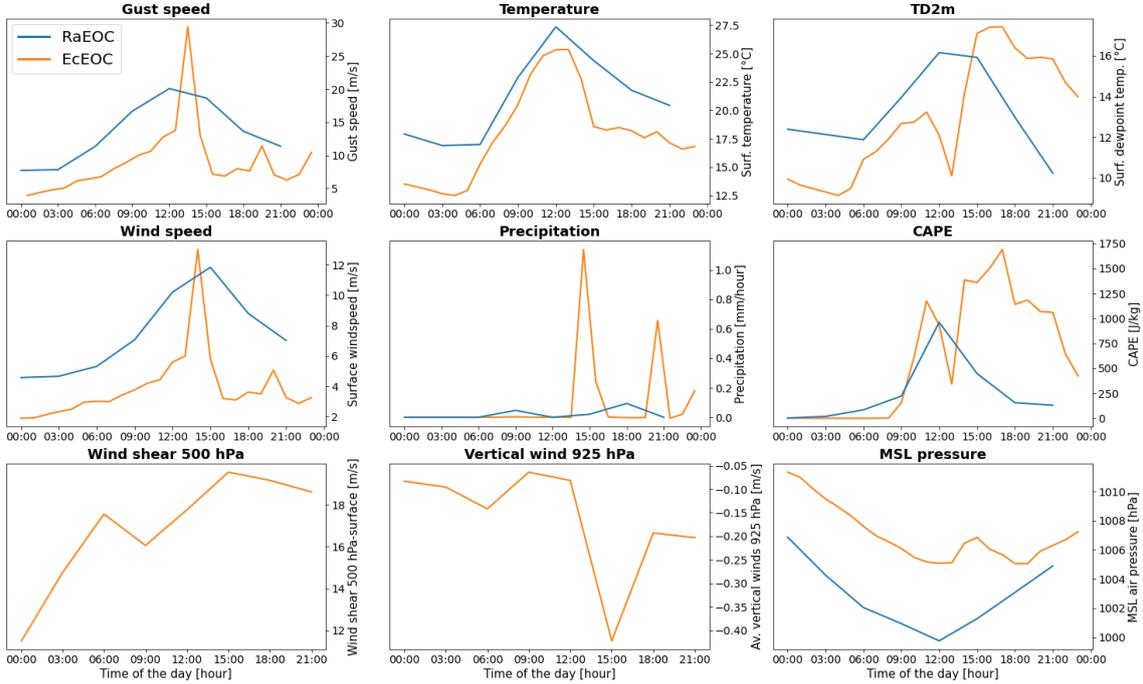
Figure 5.15: *Time series of variables of case study on the 31st of August 2099, one of the top ten maximum convective events in the RACMO run. The location of the time series is stationary and taken at the point where the gust of the event was maximum during the entire event. For HClim-EOC this was at $7.1°$ E longitude and $50.4°$ N latitude, for RACMO-EOC $3.2°$ E longitude and $51.3°$ N latitude.*

5.4.2 The RACMO's maximum events compared to the HClim cases

None of the ten maximum events of the end of century runs in HClim and RACMO happen on the same day. In fact, none except one event in August 2099 fall within the same month, and even for this month the storms are four days apart. Indeed, the physical aspects of the maximum events in RACMO are of a different type than those found in the HClim runs. First, none of the RACMO-EOC events have gust speeds above 30 m/s, in line with the boxplot of Figure 5.6. Second, most of the high gust speeds found in RACMO can be explained by the synoptic situation: most cases in RACMO are paired with strong synoptic winds and high pressure gradients associated with low pressure systems, see Figure 5.16. In all RACMO cases, the p_5 mean sea level pressure is below the p_5 for an average day, and for most events significantly (≤ 10 hPa) lower than the p_5 of a HClim case. The low pressure systems result in strong wind fields, and indeed the wind speeds of the RACMO cases are higher than most HClim cases.

Third, in none of the RACMO events the temperatures are as high as the HClim events: three locally pass $30°C$ and two reach $40°C$ for a short amount of time, locally. Related, the CAPE values of the RACMO cases are much lower than the HClim ones: the median of the p_{95} of the HClim-EOC cases is around 1800 J/kg, whereas the same value for the RACMO cases is around 700 J/kg. For the maximum CAPE value the difference is even more extreme with a median of 4700

J/kg for HClim and 1700 J/kg for RACMO. Lastly, in the animations the development of something that resembles a cold pool structure or a mesoscale convective system is absent in all the RACMO simulations. These findings show that the cases found in RACMO are more related to the synoptic situation rather than convective systems, and that the added value of CP dynamics is substantial.
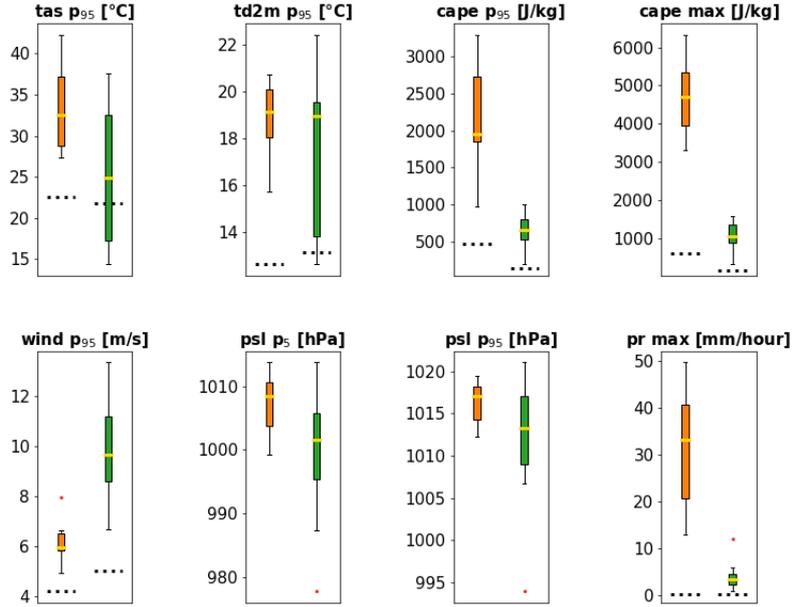

Figure 5.16: *Environmental conditions over land of 10 case studies in HClim-EOC (orange) and RACMO-EOC (green) in the Netherlands. The dotted lines represent the value of the statistics for an average summer day in the Netherlands. The boxplots are computed in the same way as Figure 5.6. Note that the psl value for an average HClim day is not available.*

Chapter 6

Discussion

6.1   Temperature bias in the EC-Earth driven HClim runs

The underestimation of most gust statistics (max, RL_{10}, RL_{50}, f_{20} and f_{25}) compared to observations is worse for HClim-hist than HClim-ERA. In addition, in the Netherlands, HClim-ERA captures around 10 summer events with gusts above 35 m/s, whereas HClim-hist only has a single event above this magnitude. The discrepancy between the EC-Earth and ERA driven run can possibly be related to a cold bias in EC-Earth. Figure 6.1 shows the mean discrepancy in surface temperature between HClim-hist and HClim-ERA in Europe. In all parts of the domain the mean HClim-ERA surface air temperature is warmer than in HClim-hist, with a larger difference over land and in southern Europe. In some regions, the bias goes up to 2.5°C.

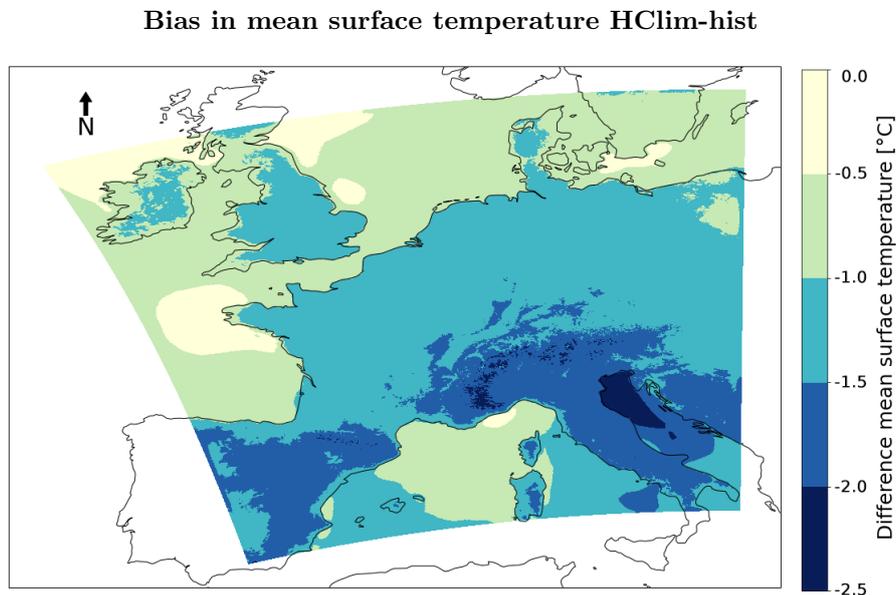**Bias in mean surface temperature HClim-hist**

Figure 6.1: *Surface temperature field averaged over all time steps of the HClim-ERA run subtracted from the HClim-hist run. Negative values thus indicate colder HClim-hist temperatures.*

To investigate whether EC-Earth is too cold or ERA too warm, temperature statistics of the models are compared to KNMI observational data between 2000-2009 at 35 stations throughout the Netherlands (see Figure 3.2). In Table 6.1 the MBE computed over the 35 locations is presented for the four Harmonie Climate runs. These results show that the mean temperature in HClim-hist is 1.58°C colder than observations, whereas HClim-ERA is only 0.49°C colder, indicating that the EC-Earth driven runs are too cold in the Netherlands.

	Temperature bias (°C)
HClim-ERA	-0.5
HClim-hist	-1.6
HClim-MOC	-0.4
HClim-EOC	1.7

Table 6.1: *Difference in mean temperature between 35 observation stations (see 3.2) hourly surface temperature data (2000-2009, all year) and 4 models extracted at the nearest grid point. Negative values indicate colder model temperatures compared to observations.*

The global mean temperature increase projected by IPCC's Fifth Assessment Report (Stocker et al., 2013) in the RCP8.5 scenario is 3.7°C between 2081-2100 relative to 1986-2005. The absolute increase compared to observations is 1.7°C by the end of the century in the HClim-EOC run, and 3.3°C relative to the HClim-hist run. The absolute increase in the model between the two periods resembles that of RCP8.5, with a projected increase of 2.6° to 4.8°C.

The increase compared to observations is better aligned with the RCP4.5 and RCP6 scenarios, with global warming increases by 2081-2100 of respectively 1.8°C (likely range 1.1° to 2.6°C) and 2.2°C (likely range 1.4° to 3.1°C) (Stocker et al., 2013). Recent studies argue that the latter two less extreme scenarios are more likely than the RCP8.5 scenario (Ho et al., 2019). Therefore, the closer resemblance of the model's end of century temperatures with the less extreme scenarios of the IPCC might be beneficial. However, a very recent report by Schwalm et al. (2020) suggests that the RCP8.5 scenario is still feasible, and therefore, the projected increase might actually be more intense than reported in this study.

The results of comparing statistics and case studies of the history and EOC run should be taken with care, as the HClim-hist temperatures are not representable for the current climate. The HClim-MOC run with temperatures similar to ERA and observations provides a better fit in terms of temperature. Indeed, when comparing the gust statistics to observations, HClim-MOC outperforms HClim-hist in most metrics. The improvement is especially significant for the maximum gust speeds and RL_{50}, with MBEs improving from -3.5 to -0.2 and -7.8 to -2.8, respectively (see table 6.2).

If the temperature bias indeed explains the differences in gust statistics between HClim-hist and HClim-ERA it would support the idea that gust magnitude is related to temperature, and that in a future warmer climate higher maxima and return levels are to be expected.

Despite the temperature biases, the comparison between the HClim-hist and HClim-EOC run still give a good indication of changes in a warming climate as the absolute temperature increase between the runs does fall within the range of the projected RCP8.5 scenario. Therefore, the differences between HClim-hist and HClim-EOC can still be taken as representation of what happens to convective gusts in a warming climate. It however remains the question what the actual effects of the temperature bias on the results are, and whether this has consequences on other variables that are pertinent to convective storms. To address this, ideally the RCMs would be forced with an ensemble of general circulation models, as already discussed at the end of section 5.1.4.

| | | HClim-ERA | | HClim-hist | | HClim-MOC | |
		RMSE	MBE	RMSE	MBE	RMSE	MBE
mean	m/s	0.4	0.0	0.4	0.1	0.4	0.1
max	m/s	3.2	-0.7	4.2	-3.5	3.1	-0.2
p_{95}	m/s	0.6	-0.1	0.6	0.2	0.6	0.0
p_{99}	m/s	0.8	-0.4	0.8	-0.3	1.0	-0.5
RL_{10}	m/s	3.1	-2.3	4.6	-4.3	2.6	-1.9
RL_{50}	m/s	5.8	-4.4	8.3	-7.8	4.5	-2.8
f_{20}	days	13.3	-10.2	16.1	-13.5	13.2	-9.5
f_{25}	days	1.5	-0.9	1.8	-1.4	1.5	-0.6

Table 6.2: *Performance statistics of modelled vs. observed summer (May to September) gusts. The observed data come from 22 inland observation stations in the Netherlands. The model data were extracted at the nearest grid points. Negative MBE values indicate a lower model magnitude compared to observations.*

6.2   Low frequency of extreme events

A second reason to take the future changes with care is the inherent low frequency of extreme events. As shown in the results the number of summer days with gusts above 25 m/s for inland Europe locally rarely exceeds one per year per grid point (Figure 5.8). When aggregating events of the entire Netherlands the number of days with inland gust speeds above 35 m/s in the entire Netherlands stays below a single event per year, even at the end of the century (Figure 5.6). For this reason, the results of extreme value analysis through the peak over threshold are not widely incorporated in this report. Coles (2001) and others suggest to use multiple decades of data, whereas for the HClim runs only 10 years is available. With short data sets the correct choice for a threshold is especially crucial, and should be done after extensive analysis. Possibly, one could aggregate the extreme events over areas of similar climatology and topography, for example guided by the spatial patterns in the 95th percentile.

Besides the relatively small data set another challenge in extreme value analysis is that the data should be provided to the algorithm into various categories depending on their physical origins. For gusts in particular this would mean that convective small gust events should be separated from larger scale frontal events. Such division can be done using event size and duration for example, as well as by taking other environmental indicators like CAPE and shear into account. The poor performance of RL_{50} of the modelled data compared to observations indeed confirm that the results of the peak over threshold analysis should be taken with care. The aggregation of data over a large area and other methods to overcome the data availability, the correct threshold choice and the binning of events into physical categories is left for future investigation.

6.3   Convective storm dynamics

The case studies have shown that Harmonie climate is able to capture mesoscale convective storms at high detail. An analysis of smaller scale storms and dynamics is challenging without 3D fields

available and the 2.5 km scale. To study the dynamics of convective downdrafts better in a warmer climate, one could perform runs at LES scales. Such studies would also help the understanding of the dynamics of tornadoes and waterspouts in convective storms in a warmer climate, as they are still too small to be resolved in the resolution of CP-RCMs. The high gust speeds found in the statistics and case studies are more related to straight line winds from downdrafts rather than rotating vortices of tornadoes and waterspouts. Another way to better examine the behaviour of events with warmer temperatures could be to look into pseudo-warming experiments. In such experiments, the current climate is forced with increased temperatures. In such runs, average changes in circulation and moisture are also taken along, but the variability is kept the same as in the historical period. It remains the question whether this latter assumption is accurate, especially for variables indicative of severe convective environments, such as shear, moisture availability and instability. Pseudo-warming experiments are available in the KNMI database, with runs of Harmonie between 2009-2019.

Note that the dynamical analysis with the case studies has been done for the Netherlands only. This region is known for its low topography, and the behaviour of convective gusts in more complex regions can significantly vary amongst geographical areas. The climatological statistics for the entire European domain show significantly higher summer gust speeds is mountainous areas, and these regions should be studied separately. In addition, the changes projected for the Netherlands do not seem as extremes as the changes for the more central part of Europe in terms of increases in maximum gust speed (see section 5.2.1), and it would be worthwhile to study cases in further inland Europe as well.

6.4   Gust parameterization and performance

Note that HClim and RACMO have used different parameterization schemes for gusts that potentially causes a discrepancy between the model results. The parameterization scheme of RACMO is in fact taking convective situations into account by adding a shear factor, whereas the parameterization of HClim does not differentiate between convective and non-convective situations. One would expect that adding a term specific for convective situation would improve the model's performance for these situations. On the other hand, the parameterization scheme of HClim does not need to be as detailed as deep convection and the outflow of showers are resolved.

However, RACMO performs significantly better when looking at the frequency of days with gusts above 20 m/s, but equally bad compared to HClim above 25 m/s. Therefore, it could be that RACMO is able to capture the less moderately severe (between 20 - 25 m/s) gusts better compared to HClim. Possibly, these events are related to shallow convection, situations that HClim is also not able to solve explicitly. As suggested by Tijm (2018) and Veen (2019), the underestimation of shallow convective storms can be improved by enhancing the model's microphysics scheme. In RACMO a convective term related to shallow shear (950 to 850 hPa) is still added, but not in HClim. It could also be that the extreme gusts in RACMO are simply spread out over a large area. Further investigation is required.

It is challenging to dissect the gust speeds of RACMO and to check the extra contribution in convective situations in this study, as the shear and the friction velocity that are required in the parameterization, are not stored. The study of Minola et al. (2020) shows that for their case the convective contribution is small, though they used a coarser model (ERA5, roughly 30 km), so a higher contribution to gusts in convective situations for RACMO is not excluded.

It would be interesting to investigate the benefits of using alternative parameterization schemes further. RACMO uses the low level (850 to 950 hPa shear) as an indication for convective systems, however, as shown by Cohen et al. (2007) shallow shear is found to be not as good as a predictor

as deep level shear (0 - 6 or 0 - 10 km) for extreme convective events. The model's performance might also improve in extreme convective situations when additional environmental indicators such as CAPE, mid-level lapse rates or vertical differences in equivalent potential air temperature are included (Cohen et al., 2007 and Minola et al., 2020).

Looking at the results and the local nature of convective gusts maxima, it is debatable whether the model would benefit from improved gust parameterization as proposed by for example Minola et al. (2020). Their and Kurbatova et al. (2018) suggestions of using hybrid parameterization schemes, that depend on whether deep convection is active or not, was also only applied to hydrostatic models. Regardless of the complexity of the gust parameterization, the model grid of RACMO is still too coarse to resolve the complex convective (cold pool) structures. To be better able in capture convective hazards, possibly a statistical post processing scheme can be used. To this end, environmental conditions indicating severe convective gusts, for example related to shear and instability, can be used to give warnings. Even though RACMO does not seem suitable for analysis of extreme gust speeds directly, the computational advantages are still large. In the future, RACMO can still be used to study changes in the environmental conditions with high potential for extreme convective gusts as seen in HClim. Such studies could resemble the work of Rädler et al. (2018) and Púčik et al. (2017), who studied increases in the number of days with high CAPE in combination with strong shear. The lack of thorough analysis into the performance of the two used RCMs for gusts specifically in relation to their parameterizations schemes shows the need for further investigation.

Chapter 7

Conclusions and Recommendations

This thesis provides an important bridge to understand the fate of convective gusts in a future warmer climate and the high potential of convection permitting (CP) regional climate models (RCMs) in such studies. It is shown that the magnitude, frequency and dynamics of convective gusts is projected to change by the end of the 21st century in Europe. The use of CP instead of hydrostatic dynamics is shown to be crucial when analysing convective gusts extremes and especially in complex terrain.

These conclusions are drawn based on a literature review and data analysis. In the literature review, the key ingredients of extreme convective gusts and their representation in RCMs is discussed. Output of the CP-RCM Harmonie Climate (HClim, Hirt and Craig, 2020) and a hydrostatic RCM RACMO (Van Meijgaard et al., 2012) forced with the general circulation model EC-Earth in a high emission scenario are used to study the effect of a warming climate on extreme convective gusts. In addition, the RCMs are forced with the global reanalysis product ERA-interim to validate the models' performance. The findings of the literature review and analysis of the modelled output are used to conclude with the following answers to the research questions.

Part A: understand key ingredients for extreme convective gusts, their projections and how convective storms can be represented in models

A1. How are convection-induced extreme gusts and their environmental indicators expected to change in a warming climate theoretically?

The main environmental ingredients for extreme gust associated with convective storms are strong wind shear and instability. Previous studies project an increase in environments with high potential for extreme convective storms in a warmer Europe (Púčik et al., 2017; Rädler et al., 2019) and United States (Diffenbaugh et al., 2013). Until now, no study has specifically examined to what extent this potential is actually utilized for increases in extreme gusts with the use of CP-RCMs.

A2. What methods can be used to parameterize gusts and how do the methods of HClim and RACMO compare?

The parameterization of HClim for gusts is based on mean wind and TKE, whereas the RACMO one is based on mean wind and friction velocity. In RACMO, an extra term related to shallow shear (950-850 hPa) is added when deep convection is active. In contrast, the HClim parameterization scheme does not take convective situations into account separately. However,

as deep convection, and consequently the outflow from thunderstorms, is explicitly resolved special consideration might not be required.

Part B: explore whether convection permitting regional climate models are effective for studying convective gusts

B1. How well are extreme convective gusts represented in HClim compared to observational data in the Netherlands?

Compared to observations HClim performs well in terms of the mean and 95th percentile summer gusts. The performance for more extreme statistics are more challenging to assess due to the low frequency and small scale nature of extreme convective gusts, but seems to be reasonable in terms of maximum gust speeds. Judging from the examination of a historical case study, HClim seems capable of capturing extreme mesoscale convective systems, but doubts are raised about smaller isolated storms as more than half of the days with gusts above 20 m/s is missed in the Netherlands. Possibly, these situations are related to shallow convective situations, where outflow from storms is not explicitly resolved. Further investigation is proposed in objective D.

B2. How does the EC-Earth forced historical HClim run perform compared to the HClim ERA-interim run?

The mean and 95th percentile gust values compare well between HClim-hist and HClim-ERA. For more extreme statistics differences between the models show. HClim-hist underestimates the maximum gust speed at almost all observation locations (MBE -3.5 m/s), whereas HClim-ERA shows a much better performance (MBE -0.7 m/s). This discrepancy can possibly be related to a significant cold bias in HClim-hist of between 1.0 and 2.5°C in Europe compared to HClim-ERA (and on average 1.6°C compared to observations in the Netherlands).

B3. Can the same results of the CP-RCM be obtained using the coarser and hydrostatic RCM RACMO?

The higher resolution HClim outperforms RACMO in two situations. First, the results show that the most extreme convective gusts are not represented by the hydrostatic RCM RACMO: in HClim, multiple events above 40 m/s are recorded whereas RACMO summer speeds do not cross 31 m/s in the Netherlands. Local convective extremes are missed and are rather smoothed out over a larger area. The higher summer gust speeds in RACMO are more related to the synoptic situation and low pressure systems rather than mesoscale convective systems. Second, the poorer performance of the coarser resolution model is especially visible in regions with increased complexity, such as the Pyrenees, the Alps and the Mistral winds of southeast France. These results show the importance of using a CP-RCM to address convective extremes, especially around complex areas, in a future warmer climate.

Part C: investigate how convective gusts will change in a future warmer climate

C1. From a climatology standpoint, how are extreme convection-induced wind gusts expected to change in a warming climate?

The HClim EC-Earth forced runs do not project significant changes in the mean and 95th percentile gust speeds throughout the Netherlands and Europe in the high carbon emission scenario. The signal of the changes is more found in the extremes. Compared to the historical run, the end of century HClim run shows an increase of 5-10 and 2-5 days (average per grid

cell, in 10 years) in the number of days with gust speeds above 20 and 25 m/s, respectively, in inland Europe. This is in agreement with aggregated statistics of the Netherlands, that also indicate an increase of summer days with high gust speeds by the end of the century. Especially in central Europe, the HClim output shows an increase in the number and size of local summer systems with extremely high gust speeds up to 45 m/s over inland Europe. In most of this region, the maximum summer gust speed is projected to increase by at least 10 m/s and up to 25 m/s locally. The area where these changes are projected correspond to areas where an increase in severe convective environments (days with strong shear, $\geq$ 15 m/s and with unstable environments, lifted index ≤ -2) is reported by Púčik et al. (2017). This should draw the attention of policy makes, as summer storms are projected to become more severe in the future, especially in central Europe.

C2. From a dynamical perspective, how are convection-induced wind gusts expected to change in a warming climate?

The cases examined in this report show that most extreme events at the end of the century are paired with extreme temperatures exceeding 40°C and up to 45°C. In addition, some events are paired with increased moisture, a combination that results in elevated instability. This combined with strong shear generates events in the HClim-EOC run that are not imaginable in the current climate. This study shows that gusts should be studied separately from precipitation, as not all extremes are paired with precipitation. The extreme winds studied in this thesis are mainly related to the straight line gust fronts resulting from mesoscale convective systems. It is not clear how well HClim is able to resolve destructive high gust speeds of tornadoes and waterspouts, and whether the dynamics of these phenomena are taken into account in the future projections. Further research is proposed.

Part D: recommend further investigation and explore what knowledge gaps remain

D1. Are there important remaining knowledge gaps regarding how extreme convective gusts might respond to climate change?

The following recommendations are made as an outlook for future work:

- Study extreme gusts separately from extreme precipitation when looking at the fate of convective storms in a warmer climate. This thesis shows that some extreme gusts are paired with little precipitation, and so separation is essential.

- Performance assessment of HClim for convective gusts in relation to its parameterization scheme in particular. In such study, one could also investigate whether HClim would benefit from an additional gust term when convection is active, in both deep and shallow convective situations.

- Study into the frequency bias and what type of events are missed by HClim. Check if they can be related to shallow convective situations, and whether this bias reduces when improving the model's microphysics scheme.

- Examine complex terrain separately. This particularly applies for the Mistral region, Denmark and mountainous regions where the projection of extreme convective gusts differs from the general story.

- The most robust change in terms of maximum wind speed magnitude is reported for central Europe. In addition to the case studies in the Netherlands, cases in Germany for example should be examined.

- More detailed analysis of the dynamical aspect of the convective storm projections using alternative data with 3D fields and vertical profiles. In addition, analyses at LES scales could give more insight into the dynamics of gusts in convective storms and their changes with increased temperatures. This is particular useful for studying the effects of climate change of very small scale but destructive phenomena such as tornadoes and waterspouts.

- Pseudo warming experiments can be deployed to investigate the effect of temperature separately. In such studies, cases of mesoscale convective systems can be analysed for their dynamics with higher temperatures.

- Recognising the usefulness of extreme value analysis, future studies can take this up in more detail by using aggregation of data over larger areas, separation of storms into physical categories, and correct threshold choices.

- If a similar experiment is to be repeated in the future, it is highly recommendable to use forcing from multiple general circulation models to draw more robust conclusions on the climatological part.

Bibliography

M. Amodei, I. Sanchez, and J. Stein. Verification of the French operational high-resolution model AROME with the regional Brier probability score. *Meteorological Applications*, 22(4):731–745, 2015.

R. A. Anthes. Introduction to parameterization of physical processes in numerical models. In *Seminar on Physical Parameterization for Numerical Models of the Atmosphere, 9-13 September 1985*, volume 1, pages 1–32, 1985.

M. Baldauf, A. Seifert, J. Förstner, D. Majewski, M. Raschendorfer, and T. Reinhardt. Operational convective-scale numerical weather prediction with the cosmo model: description and sensitivities. *Monthly Weather Review*, 139(12):3887–3905, 2011.

P. Bechtold and J.-R. Bidlot. Parametrization of convective gusts. *ECMWF Newsletter*, pages 15–18, 2009.

A. Beljaars. The influence of sampling and filtering on measured wind gusts. *Journal of Atmospheric and Oceanic Technology*, 4(4):613–626, 1987.

D. Belušić, H. de Vries, A. Dobler, O. Landgren, P. Lind, D. Lindstedt, R. A. Pedersen, J. C. Sánchez-Perrino, E. Toivonen, B. van Ulft, F. Wang, U. Andrae, Y. Batrak, E. Kjellström, G. Lenderink, G. Nikulin, J.-P. Pietikäinen, E. Rodríguez-Camino, P. Samuelsson, E. van Meijgaard, and M. Wu. HCLIM38: a flexible regional climate model applicable for different climate zones from coarse to convection-permitting scales. *Geoscientific Model Development*, 13 (3):1311–1333, 2020.

L. Bengtsson, U. Andrae, T. Aspelien, Y. Batrak, J. Calvo, W. de Rooy, E. Gleeson, B. Hansen-Sass, M. Homleid, M. Hortal, K.-I. Ivarsson, G. Lenderink, S. Niemelä, K. P. Nielsen, J. Onvlee, L. Rontu, P. Samuelsson, D. S. Muñoz, A. Subias, S. Tijm, V. Toll, X. Yang, and M. O. Koltzow. The HARMONIE–AROME Model Configuration in the ALADIN–HIRLAM NWP System. *Monthly Weather Review*, 145(5):1919–1935, 2017.

O. Brasseur. Development and application of a physical approach to estimating wind gusts. *Monthly Weather Review*, 129:21, 2001.

H. E. Brooks, J. W. Lee, and J. P. Craven. The spatial distribution of severe thunderstorm and tornado environments from global reanalysis data. *Atmospheric Research*, 67:73–94, 2003.

K. A. Browning and G. Foote. Airflow and hail growth in supercell storms and some implications for hail suppression. *Quarterly Journal of the Royal Meteorological Society*, 102(433):499–533, 1976.

A. E. Cohen, M. C. Coniglio, S. F. Corfidi, and S. J. Corfidi. Discrimination of mesoscale convective system environments using sounding observations. *Weather and Forecasting*, 22(5): 1045–1062, 2007.

S. Coles. *An introduction to statistical modeling of extreme values.* Springer, 2001.

D. Coumou, G. Di Capua, S. Vavrus, L. Wang, and S. Wang. The influence of arctic amplification on mid-latitude summer circulation. *Nature Communications*, 9(1):1–12, 2018.

W. C. De Rooy and A. P. Siebesma. A simple parameterization for detrainment in shallow cumulus. *Monthly Weather Review*, 136(2):560–576, 2008.

D. P. Dee, S. M. Uppala, A. J. Simmons, P. Berrisford, P. Poli, S. Kobayashi, U. Andrae, M. A. Balmaseda, G. Balsamo, P. Bauer, P. Bechtold, A. C. M. Beljaars, L. van de Berg, J. Bidlot, N. Bormann, C. Delsol, R. Dragani, M. Fuentes, A. J. Geer, L. Haimberger, S. B. Healy, H. Hersbach, E. V. Hólm, L. Isaksen, P. Kållberg, M. Köhler, M. Matricardi, A. P. McNally, B. M. Monge-Sanz, J.-J. Morcrette, B.-K. Park, C. Peubey, P. de Rosnay, C. Tavolato, J.-N. Thépaut, and F. Vitart. The ERA-Interim reanalysis: configuration and performance of the data assimilation system. *Quarterly Journal of the Royal Meteorological Society*, 137(656): 553–597, 2011.

M. Déqué. Frequency of precipitation and temperature extremes over france in an anthropogenic scenario: Model results and statistical correction according to observed values. *Global and Planetary Change*, 57(1-2):16–26, 2007.

N. S. Diffenbaugh, M. Scherer, and R. J. Trapp. Robust increases in severe thunderstorm environments in response to greenhouse forcing. *Proceedings of the National Academy of Sciences*, 110(41):16361–16366, 2013.

C. A. Doswell III. The distinction between large-scale and mesoscale contribution to severe convection: A case study example. *Weather and Forecasting*, 2(1):3–16, 1987.

N. Dotzek. An updated estimate of tornado occurrence in Europe. *Atmospheric Research*, 67: 153–161, 2003.

N. Dotzek, P. Groenemeijer, B. Feuerstein, and A. M. Holzer. Overview of ESSL's severe convective storms research using the European Severe Weather Database ESWD. *Atmospheric Research*, 93(1):575 – 586, 2009.

E. E. Ebert. Fuzzy verification of high-resolution gridded forecasts: a review and proposed framework. *Meteorological Applications*, 15(1):51–64, 2008.

ECMWF. *Part IV: Physical Processes.* Number 4 in IFS Documentation. ECMWF, 2009.

R. A. Fisher and L. H. C. Tippett. Limiting forms of the frequency distribution of the largest or smallest member of a sample. In *Mathematical Proceedings of the Cambridge Philosophical Society*, volume 24, pages 180–190. Cambridge University Press, 1928.

T. Fujita and R. Wakimoto. Microbursts in jaws depicted by doppler radars, pam, and aerial photographs. NASA Conference on radar meteorology. Technical report, 1983.

J. G. Galway. The lifted index as a predictor of latent instability. *Bulletin of the American Meteorological Society*, 37(10):528–529, 1956.

P. Groenemeijer and A. Van Delden. Sounding-derived parameters associated with large hail and tornadoes in the Netherlands. *Atmospheric research*, 83(2-4):473–487, 2007.

A. J. Haklander. Personal communication, 2020.

A. J. Haklander and A. Van Delden. Thunderstorm predictors and their forecast skill for the Netherlands. *Atmospheric Research*, 67:273–299, 2003.

K. E. Hanley, R. S. Plant, T. H. Stein, R. J. Hogan, J. C. Nicol, H. W. Lean, C. Halliwell, and P. A. Clark. Mixing-length controls on high-resolution simulations of convective storms. *Quarterly Journal of the Royal Meteorological Society*, 141(686):272–284, 2015.

Z. Hausfather and G. P. Peters. Emissions - the 'business as usual' story is misleading, comment on Nature.com, January 29th, 2020. URL https://www.nature.com/articles/d41586-020-00177-3.

W. Hazeleger, X. Wang, C. Severijns, S. Ştefănescu, R. Bintanja, A. Sterl, K. Wyser, T. Semmler, S. Yang, B. Van den Hurk, et al. EC-Earth V2.2: description and validation of a new seamless Earth system prediction model. *Climate dynamics*, 39(11):2611–2629, 2012.

H. Hersbach, B. Bell, P. Berrisford, S. Hirahara, A. Horányi, J. Muñoz-Sabater, J. Nicolas, C. Peubey, R. Radu, D. Schepers, et al. The ERA5 global reanalysis. *Quarterly Journal of the Royal Meteorological Society*, 146(730):1999–2049, 2020.

M. Hirt and G. Craig. Cold pool driven convective initiation: How can we improve its representation in km-scale models? In *EGU General Assembly Conference Abstracts*, 2020.

E. Ho, D. V. Budescu, V. Bosetti, D. P. van Vuuren, and K. Keller. Not all carbon dioxide emission scenarios are equally likely: a subjective expert assessment. *Climatic Change*, 155(4): 545–561, 2019.

J. R. Hosking. L-moments: Analysis and estimation of distributions using linear combinations of order statistics. *Journal of the Royal Statistical Society: Series B (Methodological)*, 52(1): 105–124, 1990.

IEA. World Energy Outlook, IEA webpage (iea.org), 2019. URL https://www.iea.org/reports/world-energy-outlook-2019.

D. Jacob, J. Petersen, B. Eggert, A. Alias, O. B. Christensen, L. M. Bouwer, A. Braun, A. Colette, M. Déqué, G. Georgievski, et al. EURO-CORDEX: new high-resolution climate change projections for European impact research. *Regional environmental change*, 14(2):563–578, 2014.

A. F. Jenkinson. The frequency distribution of the annual maximum (or minimum) values of meteorological elements. *Quarterly Journal of the Royal Meteorological Society*, 81(348):158–171, 1955.

P. A. Jiménez and J. Dudhia. Improving the representation of resolved and unresolved topographic effects on surface wind in the WRF model. *Journal of Applied Meteorology and Climatology*, 51 (2):300–316, 2012.

R. H. Johns and C. A. Doswell. Severe local storms forecasting. *Weather and Forecasting*, 7(4): 588–612, 1992.

E. J. Kendon, N. Ban, N. M. Roberts, H. J. Fowler, M. J. Roberts, S. C. Chan, J. P. Evans, G. Fosser, and J. M. Wilkinson. Do convection-permitting regional climate models improve projections of future precipitation change? *Bulletin of the American Meteorological Society*, 98 (1):79–93, 2017.

C. Kirkpatrick, E. W. McCaul Jr, and C. Cohen. Sensitivities of simulated convective storms to environmental CAPE. *Monthly Weather Review*, 139(11):3514–3532, 2011.

E. L. Kuchera and M. D. Parker. Severe convective wind environments. *Weather and forecasting*, 21(4):595–612, 2006.

M. Kurbatova, K. Rubinstein, I. Gubenko, and G. Kurbatova. Comparison of seven wind gust parameterizations over the European part of Russia. *Advances in Science and Research*, 15: 251–255, 2018.

G. Lenderink, D. Belušić, H. J. Fowler, E. Kjellström, P. Lind, E. van Meijgaard, B. van Ulft, and H. de Vries. Systematic increases in the thermodynamic response of hourly precipitation extremes in an idealized warming experiment with a convection-permitting climate model. *Environmental Research Letters*, 14(7):074012, 2019.

Y.-L. Lin. *Mesoscale dynamics*. Cambridge University Press, 2007.

C. Liu, M. W. Moncrieff, J. D. Tuttle, and R. E. Carbone. Explicit and parameterized episodes of warm-season precipitation over the continental United States. *Advances in Atmospheric Sciences*, 23(1):91–105, 2006.

P. Markowski and Y. Richardson. *Mesoscale meteorology in midlatitudes*. John Wiley & Sons, 2011.

L. Minola, F. Zhang, C. Azorin-Molina, P. A. Safaei, R. Flay, H. Hersbach, and D. Chen. Near-surface mean and gust wind speeds in ERA5 across Sweden: towards an improved gust parametrization. *Climate Dynamics*, 55(3-4):887–907, 2020.

M. W. Moncrieff and M. J. Miller. The dynamics and simulation of tropical cumulonimbus and squall lines. *Quarterly Journal of the Royal Meteorological Society*, 102(432):373–394, 1976.

V. Negro, J.-S. López-Gutiérrez, M. D. Esteban, and C. Matutano. Uncertainties in the design of support structures and foundations for offshore wind turbines. *Renewable Energy*, 63:125 – 132, 2014.

C. Normand. On instability from water vapour. *Quarterly Journal of the Royal Meteorological Society*, 64(273):47–70, 1938.

J. P. Palutikof, B. B. Brabson, D. H. Lister, and S. T. Adcock. A review of methods to calculate extreme wind speeds. *Meteorological Applications*, 6(2):119–132, 1999.

H. A. Panofsky, H. Tennekes, D. H. Lenschow, and J. Wyngaard. The characteristics of turbulent velocity components in the surface layer under convective conditions. *Boundary-Layer Meteorology*, 11(3):355–361, 1977.

V. Petoukhov, S. Petri, S. Rahmstorf, D. Coumou, K. Kornhuber, and H. J. Schellnhuber. Role of quasiresonant planetary wave dynamics in recent boreal spring-to-autumn extreme events. *Proceedings of the National Academy of Sciences*, 113(25):6862–6867, 2016.

A. F. Prein, W. Langhans, G. Fosser, A. Ferrone, N. Ban, K. Goergen, M. Keller, M. Tölle, O. Gutjahr, F. Feser, E. Brisson, S. Kollet, J. Schmidli, N. P. M. Lipzig, and R. Leung. A review on regional convection-permitting climate modeling. *Reviews of Geophysics*, (2):323–361, 2015.

A. F. Prein, C. Liu, K. Ikeda, R. Bullock, R. M. Rasmussen, G. J. Holland, and M. Clark. Simulating North American mesoscale convective systems with a convection-permitting climate model. *Climate Dynamics*, pages 1–16, 2017.

T. Púčik, P. Groenemeijer, A. T. Rädler, L. Tijssen, G. Nikulin, A. F. Prein, E. van Meijgaard, R. Fealy, D. Jacob, and C. Teichmann. Future changes in European severe convection environments in a regional climate model ensemble. *Journal of Climate*, 30(17):6771–6794, 2017.

A. T. Rädler, P. Groenemeijer, E. Faust, and R. Sausen. Detecting severe weather trends using an additive regressive convective hazard model (AR-CHaMo). *Journal of Applied Meteorology and Climatology*, 57(3):569–587, 2018.

J. Ritchie and H. Dowlatabadi. The 1000 GtC coal question: Are cases of vastly expanded future coal combustion still plausible? *Energy Economics*, 65:16–31, 2017.

A. T. Rädler, P. H. Groenemeijer, E. Faust, R. Sausen, and T. Púčik. Frequency of severe thunderstorms across Europe expected to increase in the 21st century due to rising instability. *npj Climate and Atmospheric Science*, 2(1):30, 2019.

B. W. Schreur and G. Geertsema. Theory for a TKE based parameterization of wind gusts, 2008.

C. R. Schwalm, S. Glendon, and P. B. Duffy. RCP8.5 tracks cumulative CO_2 emissions. *Proceedings of the National Academy of Sciences*, 117(33):19656–19657, 2020.

Y. Seity, P. Brousseau, S. Malardel, G. Hello, P. Bénard, F. Bouttier, C. Lac, and V. Masson. The AROME-France Convective-Scale Operational Model. *Monthly Weather Review*, 139(3):976–991, 2011.

P. Sheridan. Forecasting research technical report. Met Office Exeter, 2011.

T. F. Stocker, D. Qin, G.-K. Plattner, M. Tignor, S. K. Allen, J. Boschung, A. Nauels, Y. Xia, V. Bex, P. M. Midgley, et al. Climate change 2013: The physical science basis. 1535, 2013.

R. L. Thompson, R. Edwards, J. A. Hart, K. L. Elmore, and P. Markowski. Close proximity soundings within supercell environments obtained from the rapid update cycle. *Weather and Forecasting*, 18(6):1243–1261, 2003.

M. Tiedtke. A comprehensive mass flux scheme for cumulus parameterization in large-scale models. *Monthly Weather Review*, 117(8):1779–1800, 1989.

S. Tijm. Forecast model progress. ALADIN-HIRLAM meeting, 2018. URL `http://www.umr-cnrm.fr/aladin/IMG/pdf/20180417_fm_tijm.pdf`.

E. Van Meijgaard, L. Van Ulft, G. Lenderink, S. De Roode, E. L. Wipfler, R. Boers, and R. van Timmermans. *Refinement and application of a regional atmospheric model for climate scenario calculations of Western Europe*. National Research Programme Climate changes Spatial Planning (KvR), 2012. URL `https://library.wur.nl/WebQuery/wurpubs/427097`.

S. Vanden Broucke, H. Wouters, M. Demuzere, and N. P. M. van Lipzig. The influence of convection-permitting regional climate modeling on future projections of extreme precipitation: dependency on topography and timescale. *Climate Dynamics*, 52(9-10):5303–5324, 2019.

L. v. t. Veen. Master thesis: Current issues with modelling convective storms in HARMONIE, 2019. URL `https://dspace.library.uu.nl/handle/1874/384529`.

M. L. Weisman and J. B. Klemp. The dependence of numerically simulated convective storms on vertical wind shear and buoyancy. *Monthly Weather Review*, 110(6):504–520, 1982.

WMO. The measurement of gustiness at routine wind stations: a review, 1987. URL `https://library.wmo.int/pmb_ged/iom_31.pdf`.

Appendix A

Appendix: Model performance

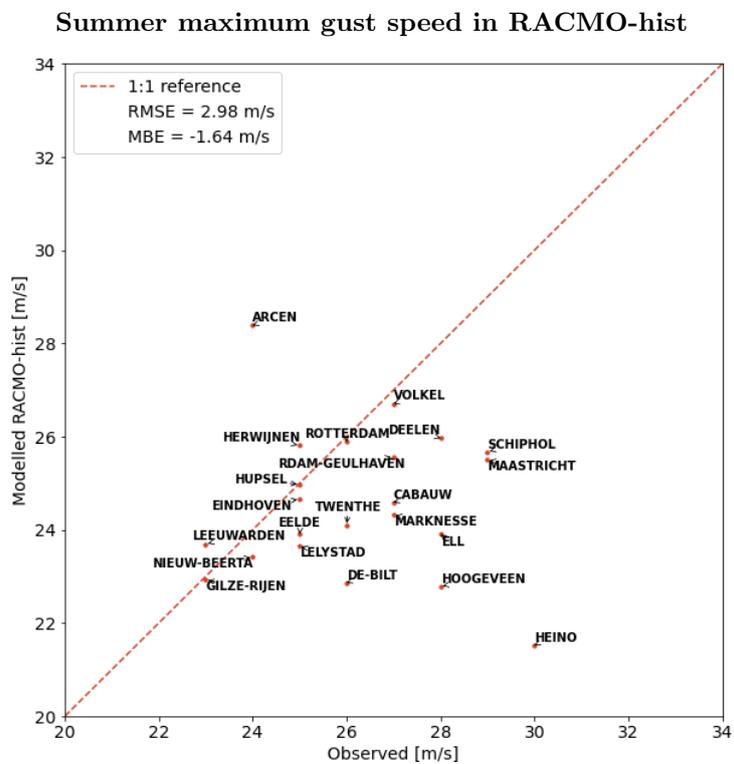**Summary maximum gust speed in RACMO-hist**

Figure A.1: *Maximum summer (May to September, all model years) gust of RACMO-hist (1996-2005) versus observations (2000-2009) at 22 KNMI station locations (see Figure 3.2).*
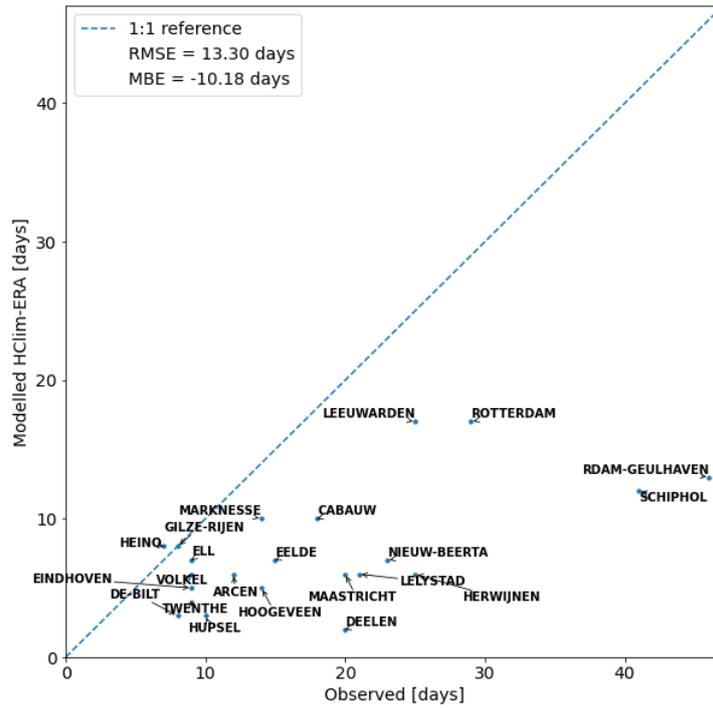
Figure A.2: *Total number of summer (May to September, all model years) days with summer gusts above 20 m/s of HClim-ERA (2000-2009) versus observations (2000-2009) at 22 KNMI station locations (see Figure 3.2).*
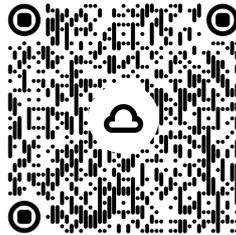
Appendix B

Appendix: External files

For this thesis a series of animations was created to simulate the maximum convective events in the model runs. These events can be found on an external drive:

External drive

If you are reading a physical copy of the report, you can also scan the following QR code:

The drive contains the following documents:

- Case studies
    1. Case June 29th 2097 (max in Harmonie Climate)
    2. Case July 24th 2091 (max in Harmonie Climate)
    3. Case August 31st 2099 (max in RACMO)
    4. Heino Case August 6th 2003 (max in observations)
    5. Additional maximum events in Harmonie Climate - EOC
    6. Additional maximum events in Harmonie Climate - history
    7. Additional maximum events in RACMO - EOC

- Model vs. Observations
    Extra figures where observations from 23 stations are compared to model data for:
    1. HClim-ERA
    2. HClim-hist
    3. HClim-MOC
    4. HClim-EOC

- Miscellaneous
    Animation of a downburst in Qatar with similar environmental conditions as the case study on June 29th 2097.